INVESTIGATION OF LASER PROPAGATION PHENOMENA
(3143-3)

The Ohio State University

ElectroScience Laboratory

Department of Electrical Engineering
Columbus, Ohio 43212

Sponsored by
Defense Advanced Research Projects Agency
ARPA Order No. 1279

Approved for public release;
distribution unlimited.

The views and conclusions contained in this document are those of the authors and should not be interpreted as necessarily representing the official policies, either expressed or implied, of the Defense Advanced Research Projects Agency or the U. S. Government.

Rome Air Development Center
Air Force Systems Command
Griffiss Air Force Base, New York

78

UNCLASSIFIED

Security Classification

DOCUMENT CONTROL DATA - R & D

(Security classification of title, body of abstract and indexing annotation must be entered when the overall report is classified)

1. ORIGINATING ACTIVITY (Corporate author)

Ohio State University
Electro Science Laboratory
1320 Kinnear Road
Columbus, OH 43212

2a. REPORT SECURITY CLASSIFICATION

UNCLASSIFIED

2b. GROUP

3. REPORT TITLE

Investigation of Laser Propagation Phenomena

4. DESCRIPTIVE NOTES (Type of report and inclusive dates)

Final Report

5. AUTHOR(S) (First name, middle initial, last name)

Stuart A. Collins

6. REPORT DATE	7a. TOTAL NO. OF PAGES	7b. NO. OF REFS
April 1972	71	25

8a. CONTRACT OR GRANT NO.	9a. ORIGINATOR'S REPORT NUMBER(S)
F30602-71-C-0132	
b. ARPA Order No. 1279	RF 3163-3
c. Program Code No. 9E20	9b. OTHER REPORT NO(S) (Any other numbers that may be assigned this report)
d.	RADC-TR-72-123

10. DISTRIBUTION STATEMENT

Approved for public release; distribution unlimited.

11. SUPPLEMENTARY NOTES	12. SPONSORING MILITARY ACTIVITY
Monitored by: Raymond P. Urtz, Jr. (OCSE) RADC, GAFB, NY 13440 AC 315 330-3443	Defense Advanced Research Projects Agency Washington, D.C. 20301

13. ABSTRACT

This report contains detailed information on the theoretical efforts of Ohio State University conducted in direct support of the RADC Laser Propagation Program. The efforts described are concentrated in three main areas: the examination of proper averaging times required for specific propagation experiments; the calculation of theoretical curves predicting results of various experiments along slant paths; and the calculation of predicted results for the temporal spectra of particular atmospheric effects.

The theoretical development and calculations have been aimed at providing useful information for comparative purposes with experimental efforts and for use by systems designers. The atmospheric effects included in the analysis are; phase structure function, angle of arrival and coherence length. Both the spatial and temporal characteristics have been considered.

1a

DD FORM 1473

UNCLASSIFIED

Security Classification

14. KEY WORDS	LINK A		LINK B		LINK C	
	ROLE	WT	ROLE	WT	ROLE	WT
Averaging Time						
Slant Path						
Outer Scale						
Temporal Spectrum						
Laser Propagation						
Coherence Length						

INVESTIGATION OF LASER PROPAGATION PHENOMENA

Stuart A. Collins

Contractor: Ohio State University
Contract Number: F30602-71-C-0132
Effective Date of Contract: 30 December 1970
Contract Expiration Date: 3 March 1972
Amount of Contract: $58,724.00
Program Code Number: 9E20

Principal Investigator: Dr. Stuart A. Collins, Jr.
Phone: 614 422-5045

Project Engineer: Edward K. Damon
Phone: 614 422-5953

Contract Engineer: Raymond P. Urtz, Jr.
Phone: 315 330-3443

This research was supported by the Defense Advanced Research Projects Agency of the Department of Defense and was monitored by Raymond P. Urtz, Jr. RADC (OCSE), GAFB, NY 13440 under contract F30602-71-C-0132.

FOREWORD

Under Contract F30602-71-C-0132, the Electro-Science Laboratory of Ohio State University has been providing direct theoretical support to experimental efforts conducted at Rome Air Development Center. Both the theoretical efforts of OSU and the experimental work of RADC have been aimed at determining the limitations of atmospheric turbulence on the propagation of laser signals for precision pointing, tracking and imaging applications. The efforts are in direct response to requirements under the ARPA Advanced Optical Image Pointing and Tracking Technology Program.

The theoretical development and analyses provided by OSU have been aimed at providing realistic predictions for the spatial and temporal behavior of propagated laser signals. Analysis of averaging time requirements has pointed the way to determining minimum time requirements for valid propagation measurements and has served to provide systems data for minimizing operational errors. The extension of theoretical predictions has proved useful in that it provides a measure of the propagation effects for cases where experimental results are difficult to obtain.

PUBLICATION REVIEW

This technical report has been reviewed and is approved.

Raymond P. Urtz Jr.

RADC Project Engineer

ABSTRACT

This report contains detailed information on the theoretical efforts of Ohio State University conducted in direct support of the RADC Laser Propagation Program. The efforts described are concentrated in three main areas: the examination of proper averaging times required for specific propagation experiments; the calculation of theoretical curves predicting results of various experiments along slant paths; and the calculation of predicted results for the temporal spectra of particular atmospheric effects.

The theoretical development and calculations have been aimed at providing useful information for comparative purposes with experimental efforts and for use by systems designers. The atmospheric effects included in the analysis are; phase structure function, angle of arrival and coherence length. Both the spatial and temporal characteristics have been considered.

CONTENTS

INTRODUCTION

This is Report 3163-3, the final technical report under Contract No. F30602-71-C-0132 entitled "Investigation of Laser Propagation Phenomena." The effort is aimed at providing theoretical support to the RADC Laser Propagation Program. The report covers the period January 1, 1971 to February 28, 1972.

The theoretical support is in the area of linear atmospheric propagation phenomena. Areas of interest include theoretical support to the performance of propagation experiments and the interpretation and processing of the data to ensure proper match between theory and experiment.

The work presented generally relates to a broader program aimed at providing basic technical information on atmospheric imaging and restoration of atmospherically degraded images, on pointing laser beams and tracking objects viewed through a turbulent atmosphere. Experiments are in progress at the Rome Air Development Center to provide the desired basic information. The work reported here first provides theoretical support for these experiments and second provides information useful to systems engineers who might use the information generated for particular applications.

This report describes in detail work performed during the past eight months of the contract. Work performed before that time will be briefly summarized subsequently.

During the past eight months work has been concentrated in three main areas: the examination of proper averaging times required for particular propagation experiments, the calculation of theoretical curves predicting results of various experiments along slant paths and the calculation of predicted results for the temporal spectra of certain recorded data. These areas will be discussed. There will also be presented a writeup on a suggested redefinition of coherence lenths.

The work on averaging times is in direct support to the RADC experimental program because it supplied procedures for the performance of effective experiments. Indeed data has been examined at RADC amd at The Ohio State University to check the recommended procedures. Further, an averaging-time meter has been built for use at RADC.

The slant path curves calculated include phase structure function and angle of arrival variance. They take into account the variation with altitude of the structure constant C_n^2, and the outer scale, L_o. These are useful for systems design studies.

The temporal spectrum calculations back up the temporal spectrum measurements being made presently at RADC. They cover the time lag spectra of the phase difference temporal correlation, log amplitude correlation, and phase correlation; and include plane and spherical waves.

Work performed during the first portion of the contract is covered in reports already distributed and in oral papers delivered. The first was the semiannual technical report (hereafter designated as (3163-2). That report covered a review of averaging time studies, a bibliography of propagation literature, and calculations of angle of arrival correlation and phase structure function for select cases where the structure parameter, C_n^2, and the outer turbulence scale varied with altitude. The second report was a study of angle of arrival fluctuations. It presented extensive calculations giving predicted variation for angle of arrival two point correlations and for large aperture angle of arrival variance. In it there was also demonstrated a coincidental identity between the two which greatly simplified calculations. There were also five oral papers presented, one (Hunt, 1971a) at the Spring Meeting of the Optical Society of America in Tuscon, Arizona, April 5-8, 1972, and the other four at the annual meeting of the Optical Society of America in Ottawa, Canada, October 5, 1971, (Wyngaard, 1971a), (Wyngaard, 1971b), (Hunt, 1971b), (Zintsmaster, 1971, 1971A).

This present report is divided into three separate sections each self-contained. The sections cover averaging times, slant path calculations, and temporal spectral calculations. In addition the report has one appendix dealing with coherence length redefinition.

REFERENCES

1. (Collins, 1971) - (ST-1), S.A. Collins, Jr. and G.W. Reinhardt, "Investigation of Laser Propagation Phenomena," The Ohio State University ElectroScience Laboratory Report 3163-2 (1971).

2. (Hunt, 1971a), P.L. Hunt and S.A. Collins, Jr., JOSA 61, 675 (1971) (A).

3. (Hunt, 1971b), P.L. Hunt, JOSA 61, 1553 (1971)(A).

4. (Lumley, 1964), J.L. Lumley, and H.A. Panofsky, The Structure of Atmospheric Turbulence, John Wiley and Sons, New York, 1964.

5. (Wyngaard, 1971a), J.C. Wyngaard, Y. Izumi, S.A. Collins, Jr., JOSA 61, 1552 (1971)(A).

6. (Wyngaard, 1971b), J.C. Wyngaard, Y. Izumi, S.A. Collins, Jr., JOSA 61, 1553 (1971)(A).

7. (Zintsmaster, 1971), L.R. Zintsmaster, JOSA 61, 1553 (1971)(A).

8. (Zintsmaster, 1971A), L.R. Zintsmaster.

I. AVERAGING TIMES

In this section we present work on averaging times for propagation data. As indicated, this work is aimed at supporting the RADC experimental program by providing means for assuring that a given data record is sufficiently long so that assumptions made in the theoretical developments are born out experimentally. Typical criteria are that time and ensemble averages be identical (the ergodic hypothesis) and that the average is independent of starting time (stationarity). The averaging times also depend intimately on the quantity being measured, fourth moments requiring longer times than second moments, and requiring different times than do spectra, etc. This work is essentially an extension of that reported in the first semiannual technical report (3163-2).

During the past eight months averaging time work has progressed in three different areas: the examination of optical phase difference data recorded at RADC, the construction of an averaging time meter to give a real-time indication of averaging time and the calculation of averaging times required for temporal spectra. These topics will now be considered.

A. Examination of RADC Data

On August 16, 1971 several runs were made measuring the phase difference at two points on an atmospherically degraded spherical wave. Data was recorded with several values of separation of the two points. The data was computer processed at RADC to remove ambiguities of π radians and analyzed at OSU to give means, variances and temporal spectra. Copies of the processed data were transmitted to OSU for examination of averaging times.

The details of the analysis are based on a previous technical report (3163-2). This procedure was applied to the data directly and to the square of the data to give the averaging times for the mean and the variance. A given section of data reduced to zero mean was divided into equal length subsections (designated by subscript, s). The variance for each subsection, B_s, was computed as was the variance for the complete section, B_N. The average of the subsection variances and the percentage difference, ε_N, between that and the complete section variance were finally calculated.

$$(1) \qquad \varepsilon_N = -\left(\frac{1}{N}\sum_{S=1}^{N} B_s - B_N\right)/B_N$$

The percentage difference was then plotted as a function of the time duration of the subsections. A typical curve is plotted in Fig. 1. When the subsection duration was too small the subsection variances tended to differ from the complete section variance. However, as the section length increased the subsection variances approached more closely

the complete section variance. When there was only one subsection, the section variance and complete section variances were identical so the last point was necessarily zero. This procedure was repeated with sections of increasing duration until a plot such as the one in Fig. 1 was obtained where the percentage deviation between the mean subsection variance and the complete section variance became very small for subsection duration much less that that of the complete section.

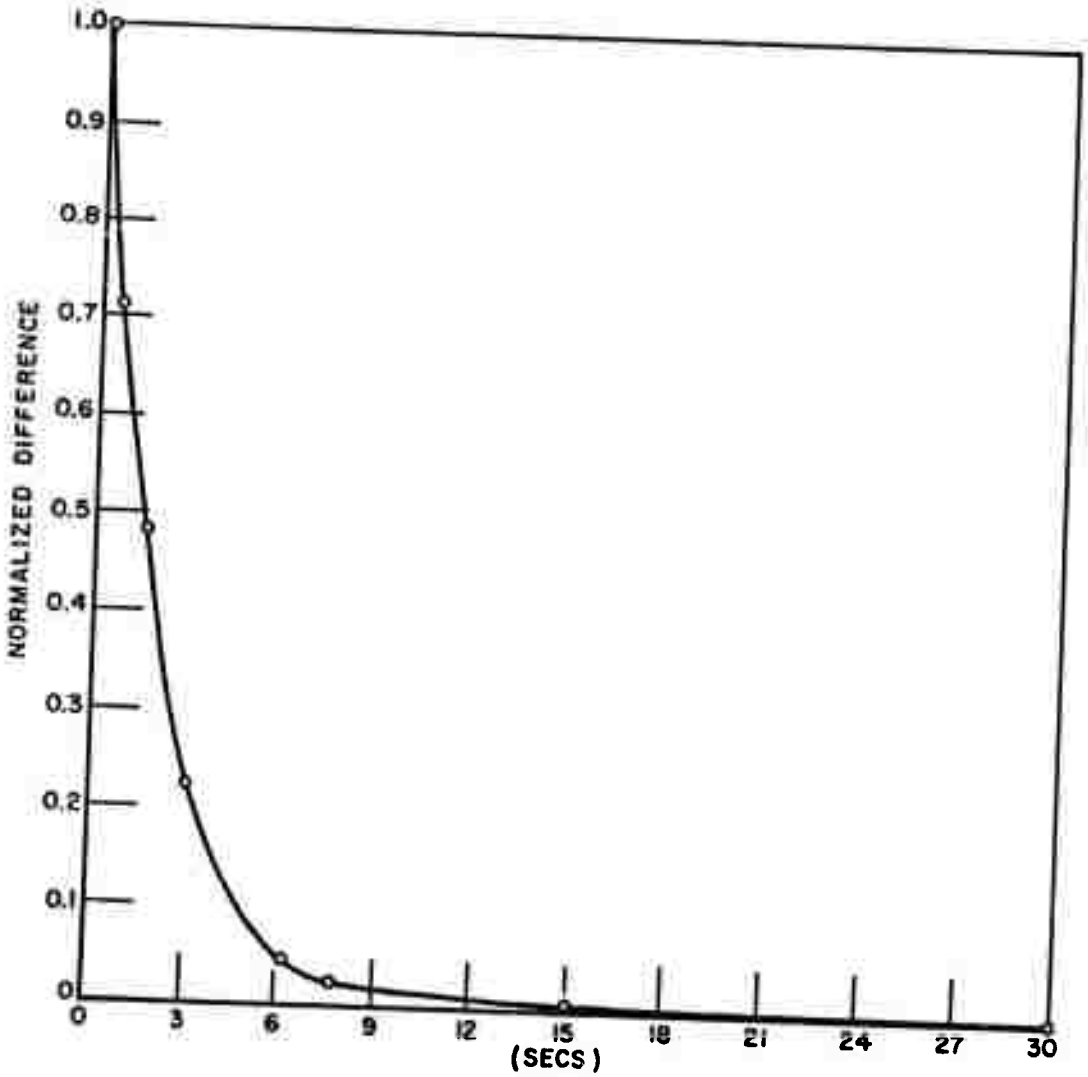

Fig. 1. Normalized difference between time and ensemble averages vs. averaging time (30 sec. record).

One would then preselect a desired degree of precision and look for the subsection duration giving the precision. That duration would then be used for all succeeding runs.

The plot in Fig. 1 has two interpretations (3163-1). The first is that the averaging time is sufficiently long that the variance of the data has come within a given fraction of the stationary value. The second is that the fractional difference between the time average value and the ensemble average value has also come within the given value.

Figure 2 shows a plot of a section of data used, redrawn from a computer printout of the digitized values. Each point represents a tenth second average. Figure 1 shows a typical plot of the percentage difference ε_N for a data section of 30 seconds duration. There it is seen that an averaging time of approximately 10 seconds would suffice for a value of $\varepsilon_N \approx .03$. This value was checked by increasing the data section duration up to as much as five minutes with the same result. Further the value was also checked by delaying the starting instant of the section with the same result. The conclusion is that for the mean value alone a ten second section of data would have been sufficient and that the variance value is stationary after that time.

The same procedure was applied to a second data section formed by squaring the original phase difference data. Figures 3 and 4 show typical plots of the percentage difference for the squared data, one for twenty and the other for one hundred and twenty seconds section duration. Both show the expected monotonically decreasing behavior. However in the longer section the normalized difference has dropped to 0.0012 in half the section duration, (60 seconds point on time scale), while the shorter record has dropped only to .04 at half section, (10 sec point of time scale) duration. Thus it appears that the averaging time of sixty seconds would be sufficient for a relative uncertainty of $.035 \simeq \sqrt{.0012}$, a value well within the five minutes of data actually recorded.

B. Averaging Time Meter

It is certainly desirable to have all data records of sufficient duration. On the other hand, excessively long data records give inefficiency. Hence it would be desirable to have some method of determining how long a data section should be while data is being taken. Towards this end two schemes have been proposed. The first is the use of an on-line digital computer to perform the calculations indicated in the previous section. The second scheme is an electronic technique to provide the same information with considerably less hardware investment. In its essence the averaging-time meter computes in analog fashion the quantities needed to determine averaging time and combines them so as to read out on a meter the requisite data duration. This averaging time meter will now be discussed.

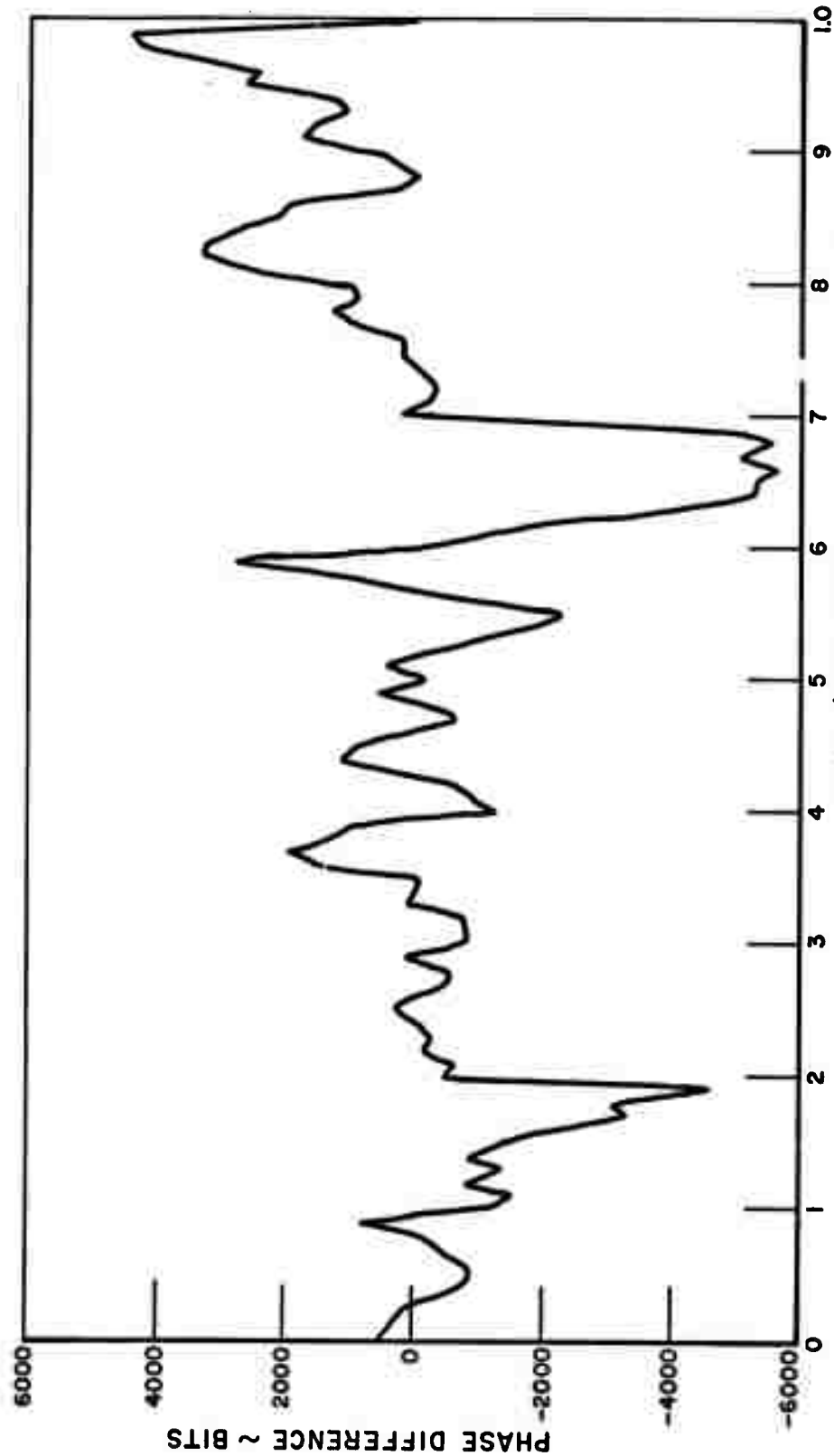

Fig. 2. Phase difference data.

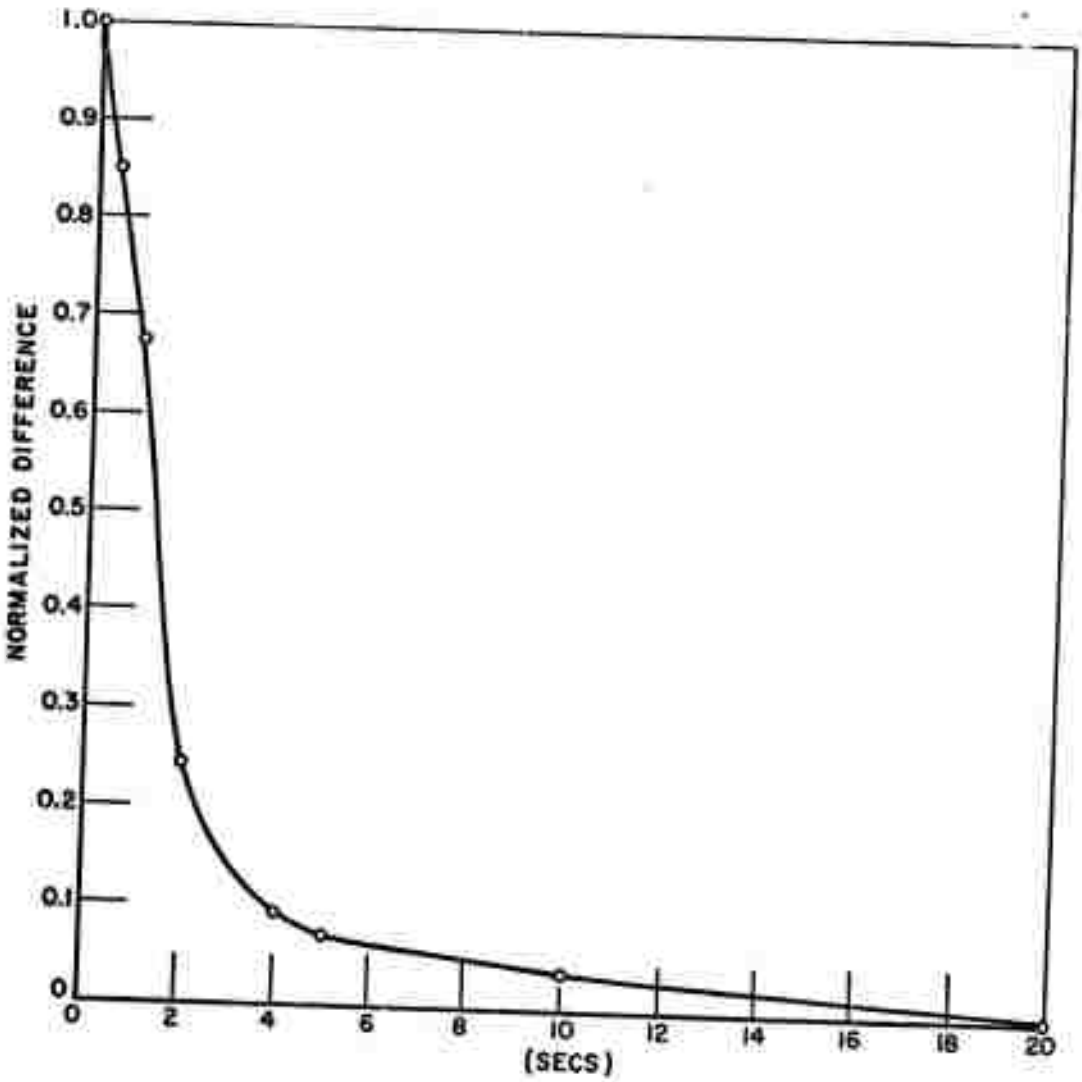

Fig. 3. Normalized difference between time and ensemble averages vs averaging time (20 sec. record).

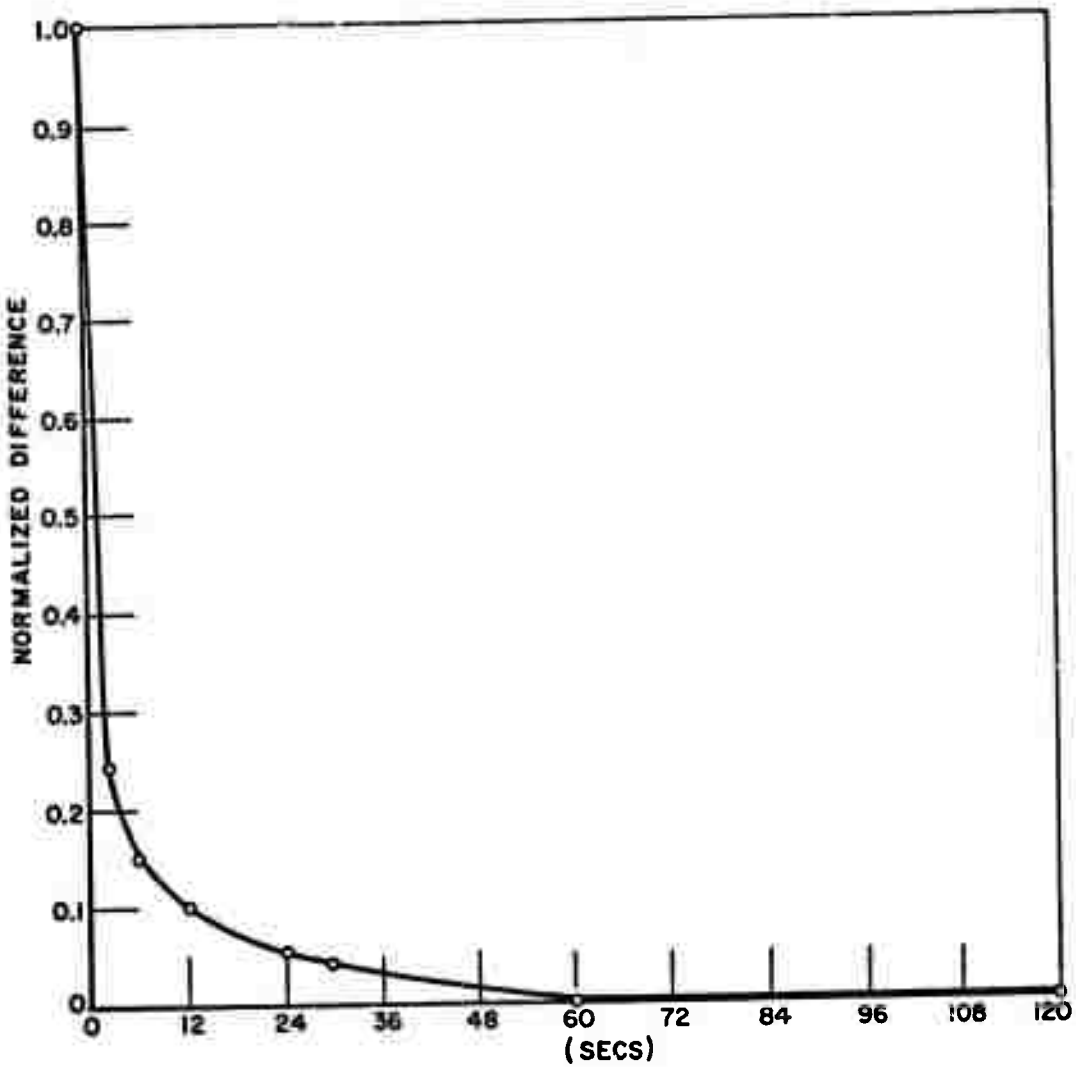

Fig. 4. Normalized difference between time and ensemble averages vs averaging time (120 sec. record).

We start with the simple equation for averaging time given in Eq. (2) (3163-1), Lumley, (1964)

$$(2)\quad T = \frac{2}{\varepsilon}\,\frac{\overline{(f-\bar{f})^2}}{\bar{f}^2}\,I$$

Where f is a random variable and ε^2 is the mean square difference between the ensemble and time averages normalized to the square of the mean value. I is the integral scale of the autocorrelation.

$$(3)\quad I = \frac{1}{B(0)}\int_0^\infty B(\tau)\,d\tau$$

$$(4)\quad B(\tau) = \overline{(f(t) - \bar{f})(f(t+\tau) - \bar{f})}$$

The restrictions in Eqs. (3) and (4) are that the averaging time be much longer than I, and that the data be normally distributed. Assuming a gaussian random process, then the averaging time is (Lumley, 1964)

$$(5)\qquad T = \frac{4}{\varepsilon^2}\,\frac{\int_0^\infty B(\tau)d\tau}{B(0)}$$

In terms of frequency integrals rather than time domain integrals Eq. (5) becomes

$$(6)\quad T = \frac{2\pi\, W(0)}{\varepsilon^2 \int_0^\infty W(f)df}$$

Equation (6) contains the ratio of two power levels, the power at DC and the broadband power. Thus the problem becomes one of measuring these two quantities. The block diagram of a circuit for accomplishing this is shown in Fig. 5. There we see the signal entering at the left and split into two parallel paths. The top path squares the signal and then integrates it to obtain the average power. This implements the denominator of Eq. (6). In the bottom string the signal is integrated to give the average signal which is then squared to give the average DC power corresponding to the numerator. The logarithms of the two signals are then subtracted to obtain a voltage proportional to the log of the averaging time. A meter with a log scale is used to read out the averaging time directly.

The circuit indicated in Fig. 5 has been constructed and is shown in Fig. 6 but it has yet to be tested. Tests are expected with the same random signals used for the analysis in the preceding section.

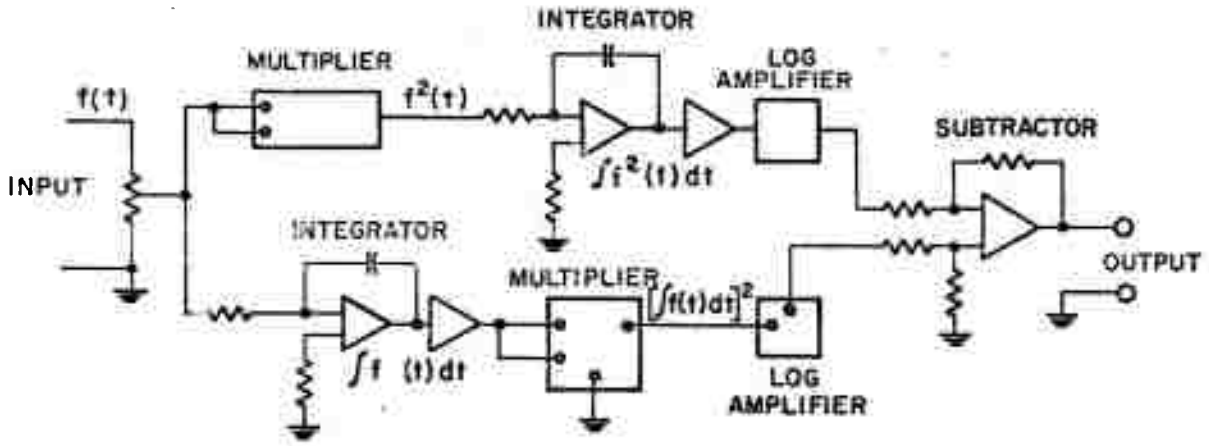

Fig. 5. Averaging time meter circuit.

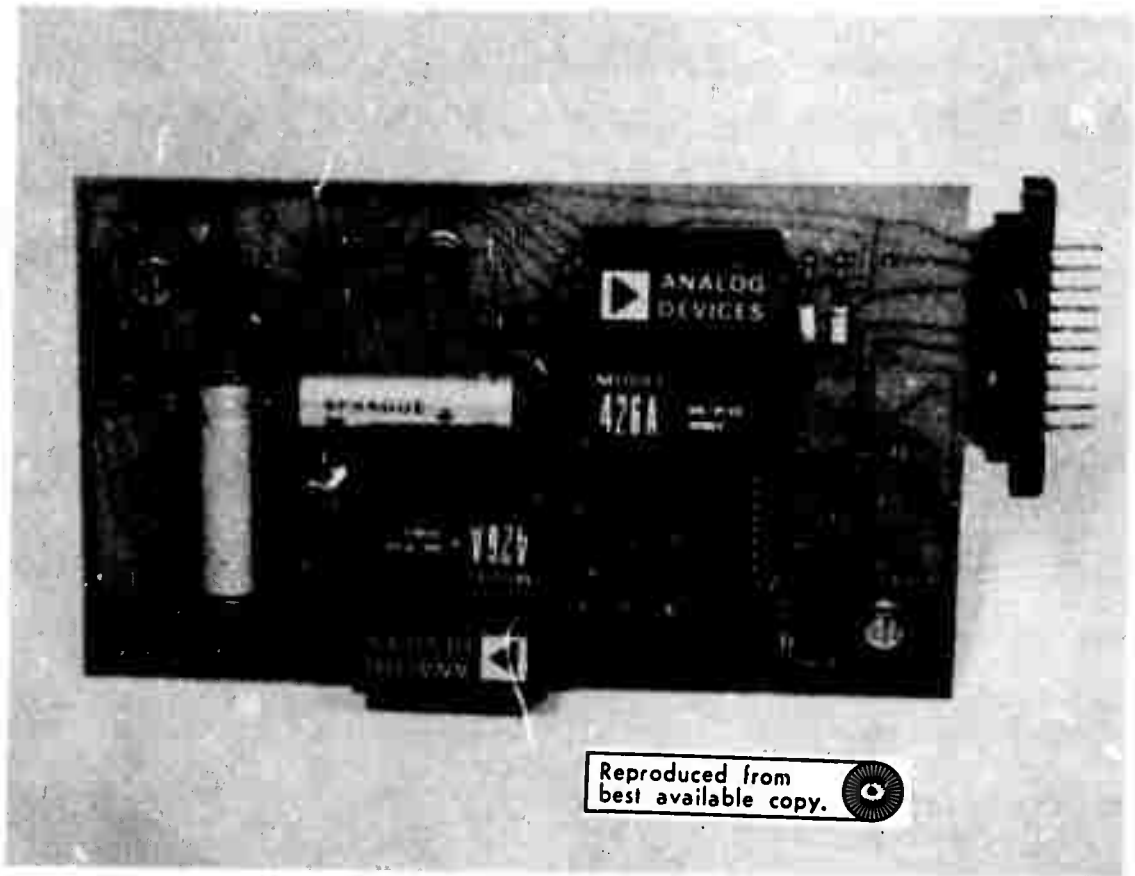

Fig. 6. Circuit board for averaging time meter.

C. Temporal Spectra Averaging Times

It is of interest to examine the temporal spectra of random data as well as the time averages. Indeed Section III of this report contains analytical predictions for the form of the temporal spectra of log-amplitude, phase and phase difference fluctuations for turbulence-degraded light beams. It is the object of this subsection to consider one averaging time prediction procedure (Blackman, 1958) as applied to phase difference temporal spectra. The prediction will then be interpreted to show that it provides one limitation on averaging times, but not necessarily the desired limitation.

The discussion is based on the expression for power spectral averaging times found in the literature (3163-1), (Blackman, 1958). The pertinent expression is

$$(7)\quad T_n' = \frac{2}{\varepsilon^2 W_e}$$

where

$$(8)\quad W_e = \frac{\left[\int W(f)df\right]^2}{\int W^2(f)df}$$

T_n' is the required averaging time, ε^2 is the relative mean square uncertainty in the power spectral measurement and W_e is a mean effective bandwidth. Analytical expressions for the power spectra for various propagation variables are calculated in Section III. These can be used to obtain analytical estimates for the mean bandwidth and therefore the averaging time using Eqs. (7) and (8). We present such a calculation for a typical case of interest, phase difference measurement.

For phase difference measurements the power spectrum $W_{\delta s}(f)$ is predicted in Section III to have the form

$$(9a)\quad W_{\delta s}(f) = K \cdot X^{-8/3}\left[1 - \frac{\sin X}{X}\right]\left[1 + \left(\frac{R}{X}\right)^2\right]^{-4/3}$$

where

$$(9b)\quad K = .033 \times (2\pi)^{8/3} \times \left\{\begin{matrix}1\\2\end{matrix}\right\} \times k^2 L\, C_n^2\, \rho^{8/3} v$$

$$(9c)\quad X = 2\pi f \rho / v$$

$$(9d)\quad R = 1.077\rho / L_o$$

ρ is the phase measurement point separation, v is the wind component velocity parallel to ρ, L_o is the turbulence outer scale, C_n^2 is the turbulence structure parameter, and $\lambda = 2\pi/k$ is the light wavelength.

To give a simple approximate estimate of the predicted averaging time the expression in Eq. (9a) was replaced by its limiting values in three different regions,

$$(10)\quad K = X^2/6R^{8/3} \qquad 0 \leq X \leq R$$
$$= X^{-2/3}/6 \qquad R \leq X \leq 6$$
$$= X^{-8/3} \qquad 6 \leq X$$

and the integrations indicated in Eq. (8) were performed. The resulting expression for W_e is given by

$$(11)\quad W_e^{-1} = (2\pi\rho/v)\left[\frac{\frac{4R^{-1/3}}{45} - \frac{6^{-1/6}}{13}}{\left(\frac{6^{7/6}}{10} - \frac{4}{9}R^{1/3}\right)^2}\right]$$

W_e^{-1} normalized to ρ/v is plotted in Fig. 7. Using Eq. (9d) and Fig. 7, we see that for ρ/L_o in the range $.01 < \rho/L_o < 1.0$, $W_e^{-1}/(\rho/v)$ is in the range $1 < W_e^{-1}/(\rho/v) < 5$. If we take representative values for separation and wind velocity, v = 15 mph ($\approx$7.2 m/s) and ρ = 0.5 m and ε = 0.1, then the range of values for the decorrelation time, W_e^{-1}, is between .066 and .33 seconds, and the averaging time is between 13.3 and 66 seconds. The frequency resolution consistent with the desired precision goes from 3.0 to 15.0 Hz.

Equation (7) gives an averaging time based on one criterion which may not be the best for all situations. Specifically it is based on the decorrelation time and not on desired spectral resolution. In many cases the spectral resolution requirement will be the more strict one requiring longer data duration than predicted by Eq. (7).

To see the decorrelation time limit, imagine that we start with a section of data T seconds in duration and calculate the associated spectrum. It will have a resolution of 1/2T Hz. Since the data is random there will probably be scatter in the frequency spectrum points. We could then group adjacent points together and average within a group to reduce the scatter. This increases the effective frequency bandwidth by the uncertainty principle that is roughly equivalent to dividing the data section into subsections, finding the spectrum of each subsection and averaging the subsection spectra.

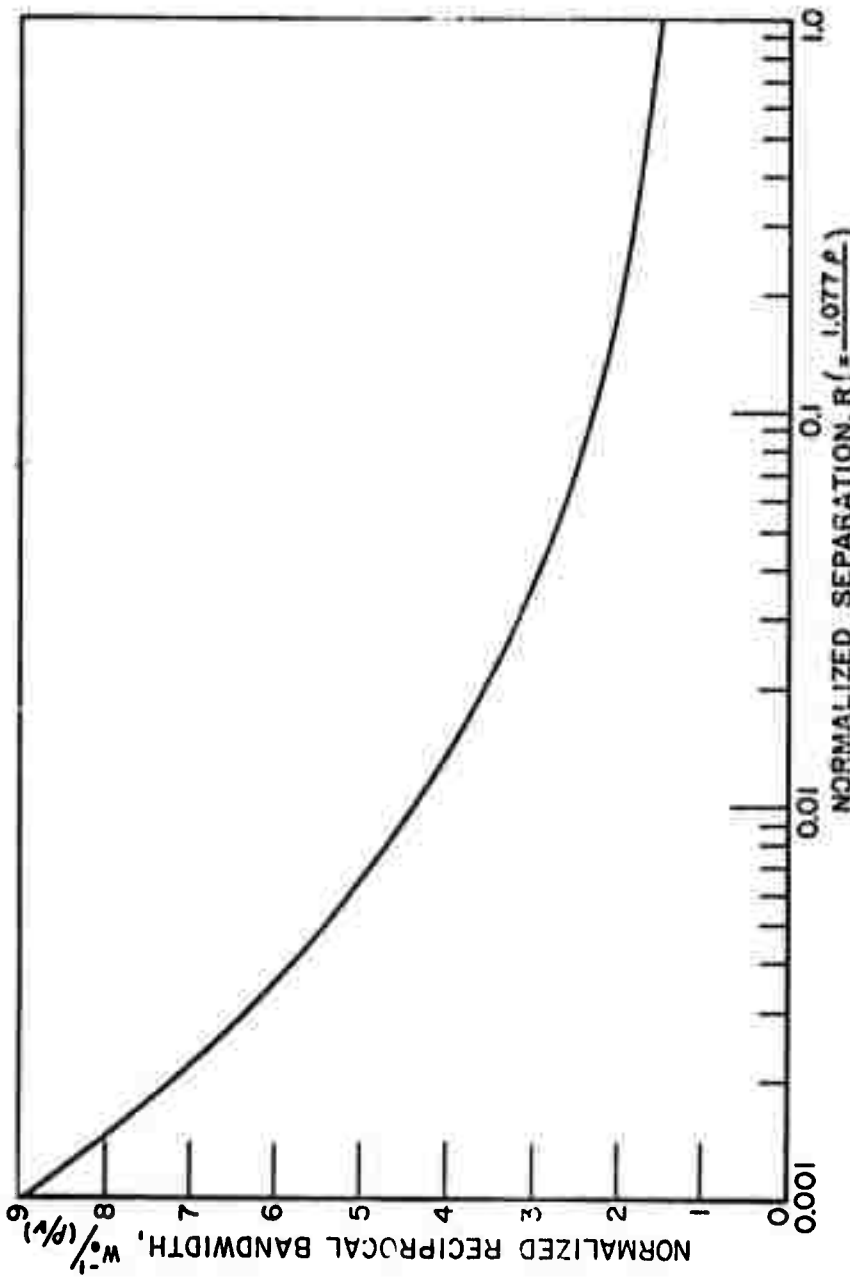

Fig. 7. Normalized reciprocal bandwidth as a function of the normalized separation.

The interpretation of W_e is that is provides a limiting largest bandwidth. It will do no good grouping spectral points with a bandwidth larger than W_e because the individual points would be no longer independent. That is, grouping the data points into a larger frequency interval would be equivalent to dividing the time data section into subsections each shorter than the correlation time, and therefore into subsections which are no longer independent.

If better frequency resolution is desired with scatter reduced, then a longer section of data must be used to provide a greater density of points in the spectrum and hence groups of smaller bandwidth but the same scatter. As indicated this is more apt to be the limiting factor on averaging time than is the coherence time limit indicated in Eq. (7).

As an example, in the case considered, if it is desired examine frequencies below 1.0 Hz, than a 0.1 Hz resolution would be more appropriate than the range 3.0 to 15 Hz cited. One must go to a data section of 33 min. duration and group to provide more spectral points to average.

Summary

To summarize the results of this section: three areas associated with averaging time have been considered. In the first area, an examination of a section of RADC propagation data on phase difference fluctuations indicated that sufficiently long averaging times had been chosen. In the second area, a real time averaging time meter had been designed and constructed. In the third area it was indicated that the limitation on averaging time for spectral data was probably the spectral resolution desired rather than the percentage uncertainty required.

REFERENCES

1. (Blackman, 1958), Blackman, R.B. and J.W. Tukey, The Measurement of Power Spectra, Dover Publications, New York, 1958.

2. (3163-2) - S. A. Collins, Jr. and G.W. Reinhardt,"Investigation of Laser Propagation Phenomena," The Ohio State University ElectroScience Laboratory Report 3163-2 (1971).

II. SLANT PATH CALCULATIONS

A. Introduction

This section is concerned with the propagation of spherical waves along slant and vertical paths through the turbulent atmosphere, and specifically with the phase structure, wave structure, and angle of arrival correlation functions for light propagated along slant paths.

The phase structure function is of interest because it is a measure of the distortion of the simple phase of a wave and is the starting point for calculating the angle of arrival statistics. The wave structure function is used in determining the modulation transfer function of the turbulent atmosphere which leads to determination of transmitted image quality and focused spot size. The angle of arrival correlation functions are important in determining tracking error of a distant source.

Similar calculations were reported previously for spherical and plane waves propagating along a horizontal rather than slant path.[1,2] However many interesting practical applications and even some of the experimental ranges involve slant or vertical paths. Spherical wave calculations are used because a spherical wave model more often approximates the light from finite sized laser sources for the longer propagation paths than do the infinite plane wave equations. The curves will show the significant difference between upward and downward propagation along the same path and the large variation in differential contribution to beam degradation along the path.

Part B shows the nondimensionalized equations for the phase structure function, angle of arrival correlation functions and angle of arrival variance for slant paths, and Part C presents typical curves obtained by numerical integration. Part D is a brief summary of the calculations and Part E a statement of the important conclusions.

B. The Theory

Spherical wave phase structure for a locally homogeneous isotropic medium[3] is given by

$$(1) \qquad D_s(\rho) = 8\pi^2 k^2 \int_0^\infty (1-J_0(\kappa\rho))\kappa \, d\kappa \times \int_0^L \left(\frac{L}{\eta}\right)^2 \cos^2\left[\frac{L(L-\eta)\kappa^2}{2k\eta}\right] \Phi_n(\kappa,\eta,L)\, d\eta,$$

where ρ is the separation of the points under consideration

k is source wave number in the unperturbed medium = $\frac{2\pi}{\lambda}$

L is the range

κ is the spatial frequency

Φ_n is the index of refraction structure function.

The phase structure function equation is simply changed to the wave structure function $D_w(\rho)$ by removing the cosine squared term in Eq. (1).

In the case of the larger separations the cosine term does not differ from unity during the significant part of the integration, then the phase structure function equals the wave structure function. For small separations, the cosine term oscillates rapidly during the significant part of the integration and $D_s(\rho/L_o)$ is 1/2 $D_w(\rho/L_o)$. This is identical to the conclusion for the plane wave case.

The elevation angle of arrival correlation function is related to the phase structure function by[4]

$$(2a)\quad B_\alpha(\rho) = \frac{1}{2k^2} \frac{\partial^2 D_s(\rho)}{\partial \rho^2}$$

and the azimuth angle correlation function by[5]

$$(2b)\quad B_\beta(\rho) = \frac{1}{2k^2\rho} \times \frac{\partial D_s(\rho)}{\partial \rho} \quad .$$

The angle of arrival variance is

$$(2c)\quad B_\alpha(0) = B_\beta(0).$$

The Von Karman Index spectrum[6,7] including inner scale is

$$(3)\quad \Phi_n(\kappa,\eta,L) = .033\, C_n^2(\eta) \frac{e^{-\left(\frac{\kappa L}{\eta} \frac{\ell_o}{5.92}\right)^2}}{\left(\left(\frac{\kappa L}{\eta}\right)^2 + \left(\frac{1.077}{L_o}\right)^2\right)^{11/6}} \quad .$$

$C_n^2(\eta)$ is the index of refraction structure constant.

ℓ_o = inner scale of turbulence

L_o = outer scale of turbulence.

A recent paper[8] has determined by semiempirical theory and direct experimental verification that

$$(4) \qquad C_n^2(\eta) = C_n^2(H_o)\, H(\eta)^{-4/3}$$

where $H(\eta)$ is path altitude divided by the initial altitude H_o. The outer scale varies linearly with altitude[9]

$$(5) \qquad L_o(\eta) = L_o(H_o)\, H(\eta)$$

We now convert to dimensionless variables. The nondimensionalized calculations allow their use for a large variety of situations and illustrates the beginning of a more comprehensive understanding of turbulence calculations, by accentuating pertinent combinations of experimental quantities. The new variables are

$$(6) \qquad u \equiv \kappa L_o(H_o) \qquad \gamma = \frac{2k[L_o(H_o)]^2}{L}$$

$$\nu \equiv \eta/L \qquad \gamma' = \frac{2k[L_o(H_L)]^2}{L}$$

$$\beta = \frac{H_L - H_o}{H_o} \qquad H(\eta) = (1 + \beta\nu)$$

where H_L is the altitude at the receiving end of the path. This simplifies the integrals and emphasizes the range and initial outer scale dependence of the turbulence statistics. Then

$$(7) \qquad D_s(\rho/L_o(H_o)) = .033 \times 8\,\pi^2\, C_n^2(H_o)\, L_o(H_o)^{+5/3}\, k^2 L$$

$$\times \int_0^\infty du \left(1 - J_o\left(\frac{u}{L_o(H_o)}\,\rho\right)\right) u$$

$$\times \int_0^1 d\nu \; \frac{(1+\beta\nu)^{-4/3}}{\nu^2} \cos^2\left(\frac{u^2(\nu-1)}{\gamma\nu}\right)$$

$$\times \left(\left\{\frac{1.077}{1+\beta\nu}\right\}^2 + \left(\frac{u}{\nu}\right)^2\right)^{-11/6}$$

The angle of arrival correlation functions are easily derived from the phase structure function using Eqs. (2a), (2b), and (7).

C. Computer Generated Curves

These calculations have been performed on an IBM model 360 computer using double precision arithmetic, and 96 point gaussian quadrature numerical integration.

Figure 1 shows the normalized spherical wave phase structure function computed from Eq. (7) for an upward path for two H_L/H_o ratios.

The curves show very little saturation as is the case for infinite outer scale, because the expanding upward beam sees an ever increasing L_o, so that a characteristic beam width is generally less than the local outer scale. For inner scales less than a few centimeters the exponential term of Eq. (7) is essentially unity and therefore inner scale effects are not included in the phase structure function calculations.

As an example of the use of this figure consider a 10μ spherical wave source propagating along a 45° upward slant path starting at an elevation of 1 meter and ending at an elevation of 100 meters ($L \doteq 140$m). Further assume that the initial outer scale (L_o) is 2 meters and C_n^2 is 10^{-14} $m^{-2/3}$ at one meter altitude. Choose ρ = 1 meter . Hence the normalization factor $k^2 C_n^2(H_o) L_o^{5/3}(H_o) L$ is 1.76. From the graph for H_L/H_o = 100 and ρ/L_o = 1/2 we get 1.2×10^{-3} and calculate $D_s(1\text{ m}) = 2.11$. If the path is lengthened so that H_L = 1000 m (L = 1414) then $D_s(1\text{ m}) = 106$.

A similar computer calculation for a downward slant path is shown in Fig. 2, where the curve has been renormalized to the receiver altitude.

Figure 3 shows the differential path contribution for H_o/H_L = 1000 for the case considered in Fig. 2. There we see a large contribution to the phase structure at the lower altitudes (end of downward path).

When the calculations of Figs. 2 and 3 are extended to large $\frac{\rho}{L_o(H_L)}$ values, the normalized phase structure function curve saturates like the horizontal path curves saturate, and the differential path contribution curve shows a more rapid increase near the transmitter end than at the receiver end just as in the horizontal path case. The data for large $\rho/L_o(H_L)$ are not included because they are beyond the range of importance for practical applications.

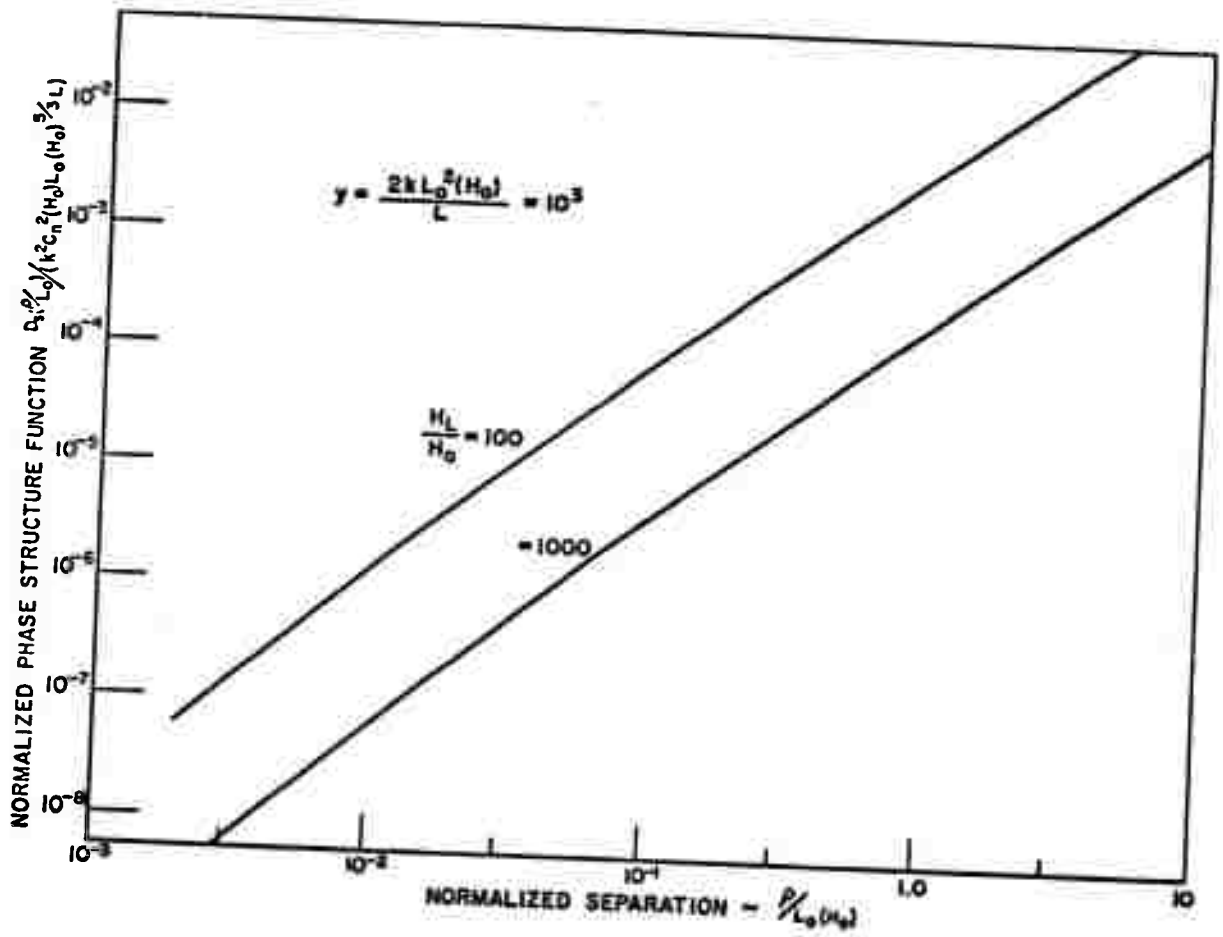

Fig. 1. Normalized spherical wave phase structure function vs normalized separation for an upward path.

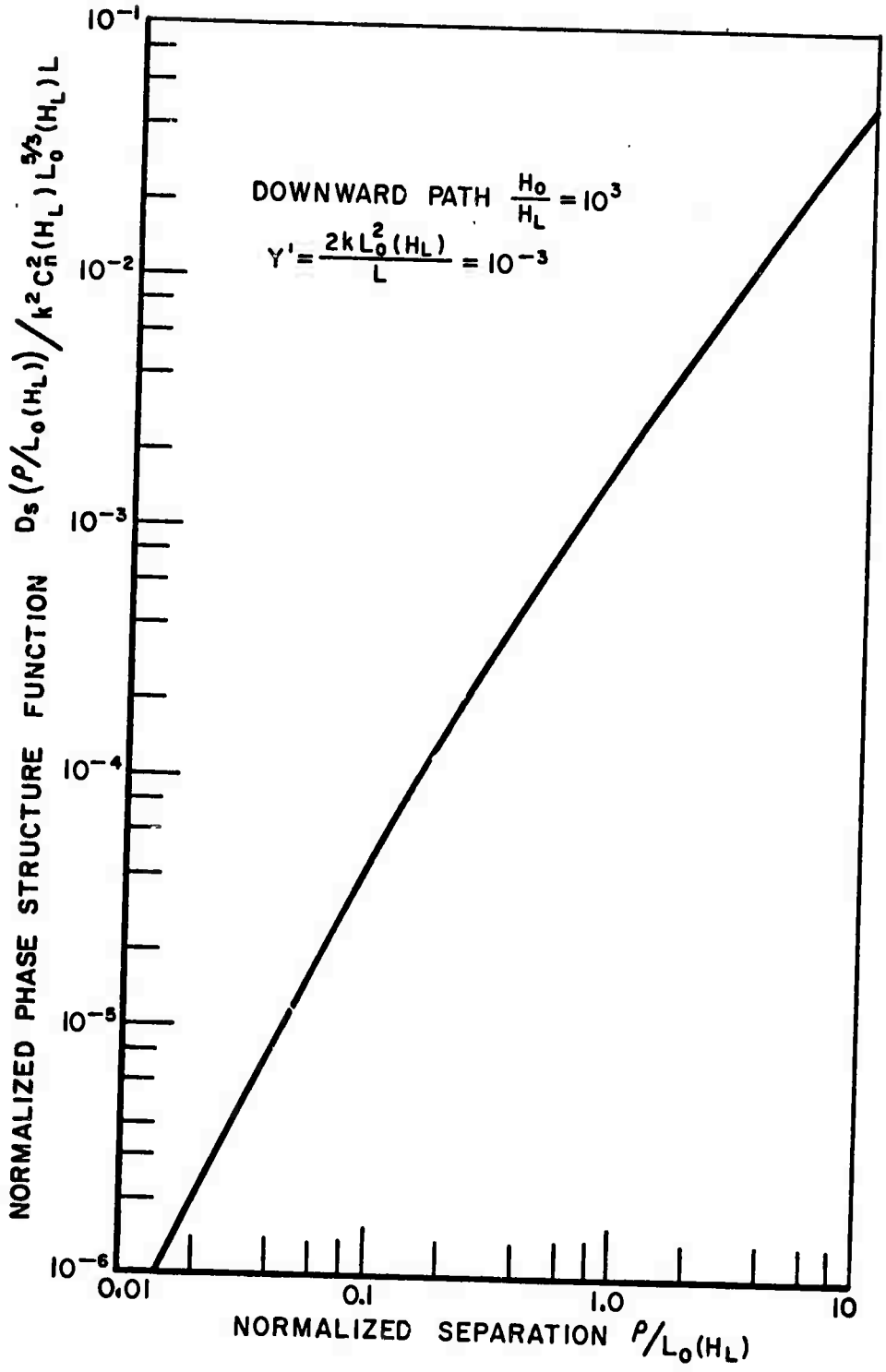

Fig. 2. Normalized spherical wave phase structure function vs normalized separation for a downward path.

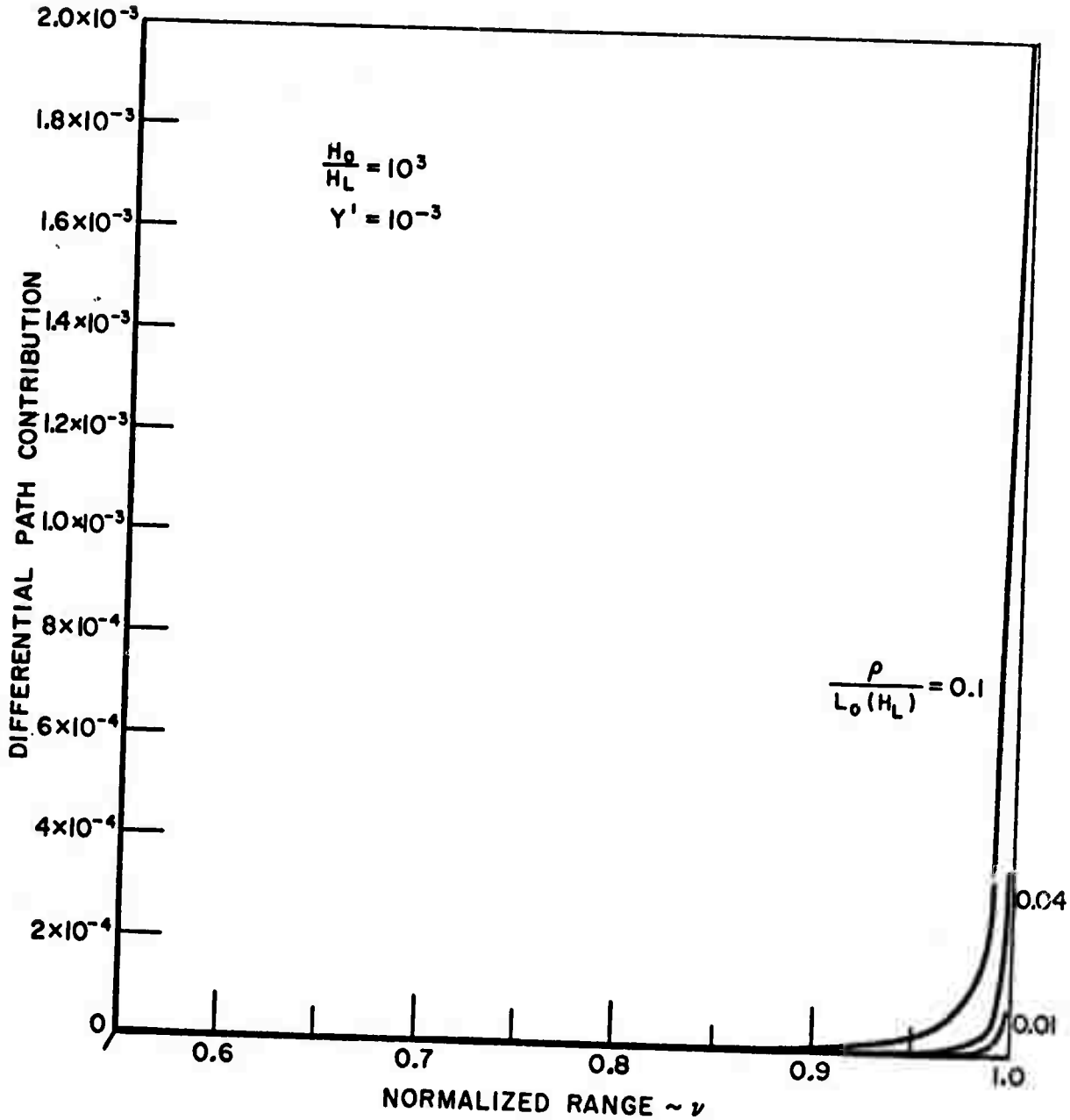

Fig. 3. Differential path contribution to spherical wave phase structure function for a downward path.

Figure 4 illustrates the small aperture azimuth angle of arrival correlation function[9] or large aperture arrival angle variance for inclined and horizontal paths and Fig. 5 shows the same calculation for a vertically downward path. The 5.005 km initial altitude is greater than the limits set by Reference 6, but the equation is correct in the lower altitudes where the major contribution to the result is made and it is a reasonable extrapolation at the higher altitudes.

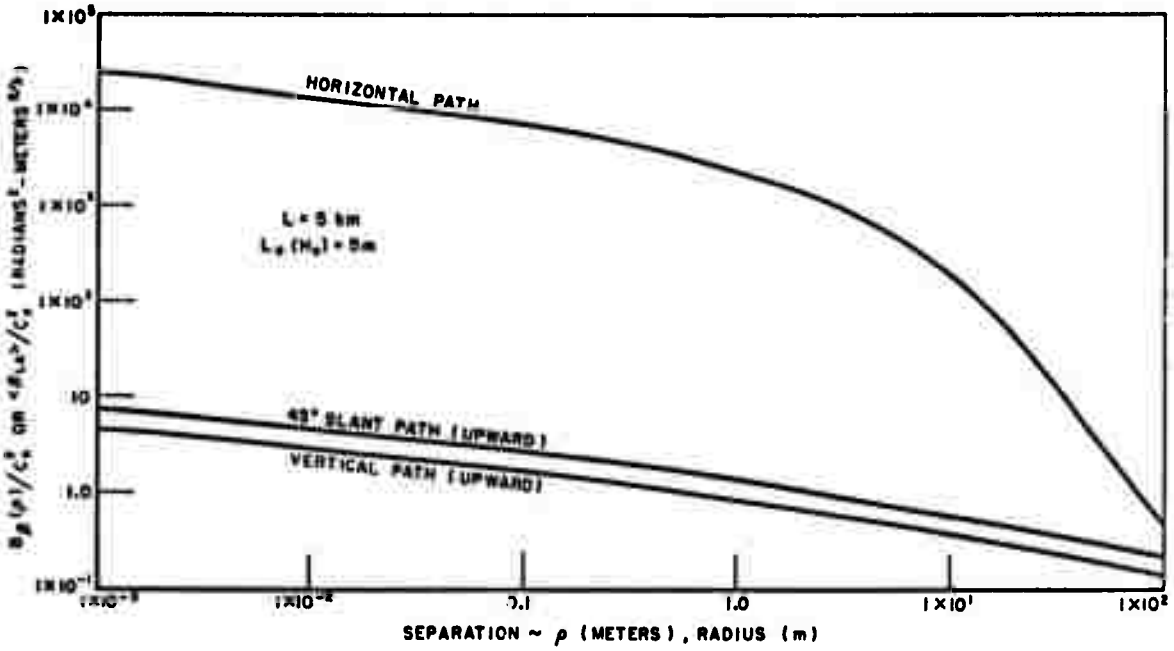

Fig. 4. Spherical wave small aperture azimuth angle of arrival correlation vs separation and large aperture mean square angle of arrival vs aperture radius.

Figure 6 shows the angle of arrival variance for a slightly inclined path. The $L^{-1/3}$ dependence can be determined analytically by dropping all but the most significant terms in the integral expression obtained by using Eq. (3) and (1) in Eq. (2b).

D. Summary

Typical examples of the slant path spherical wave phase structure function, azimuth angle of arrival correlation function and angle of arrival variance have been calculated.

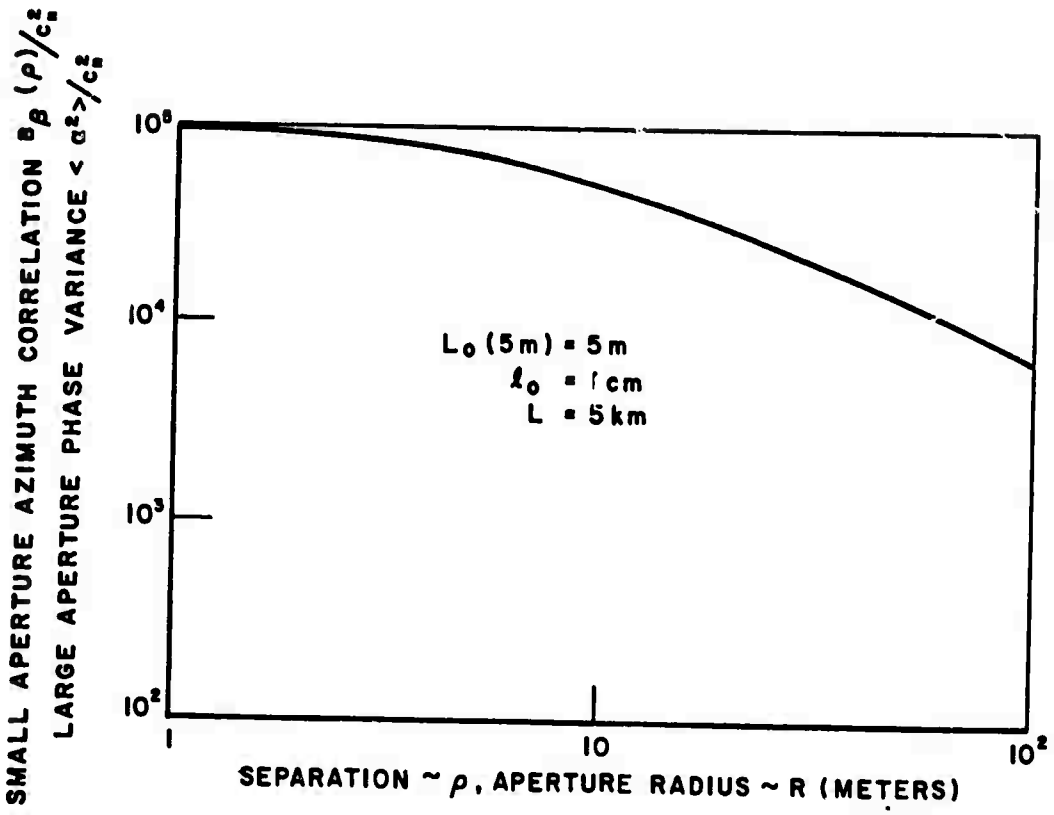

Fig. 5. Spherical wave small aperture azimuth angle of arrival correlation vs separation and large aperture mean square angle of arrival vs aperture radius for vertical downward path.

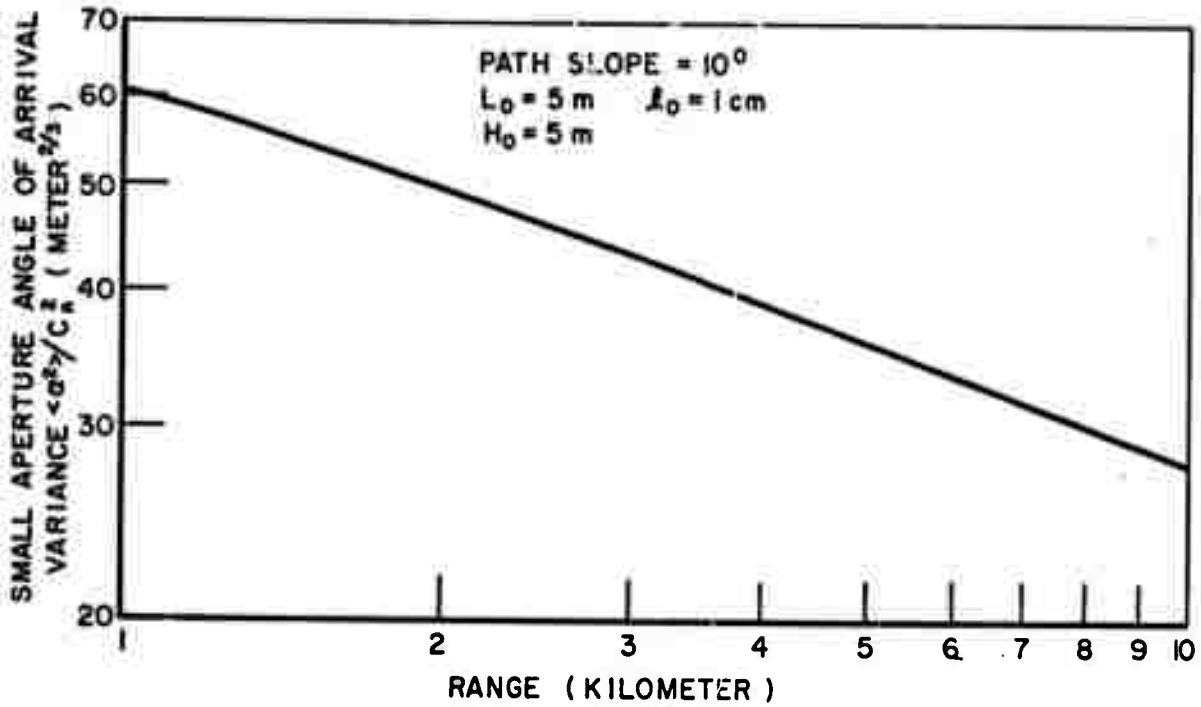

Fig. 6. Small aperture angle of arrival variance vs range for an upward slant path.

E. Conclusions

The variation of the turbulence statistics with elevation show that a substantial decrease in turbulence effects can be achieved by avoiding the lower atmosphere especially for the downward paths.

These calculations show that altitude effects on the size of turbulence effects are very important and can not be neglected. The calculations also show the nonreciprocity of spherical wave propagation along slant and vertical paths.

REFERENCES

1. Zintsmaster, L. R., "Angle of Arrival Calculations at 10.6μ," Report 3163-1, June 1971, The Ohio State University ElectroScience Labotatory, Department of Electrical Engineering; prepared under Contract F30602-71-C-0132 for Rome Air Development Center. (RADC-TR-71-124).

2. Collins, S. A., Jr. and Reinhardt, G. W., "Investigation of Laser Propagation Phenomena," Report 3163-2, August 1971, The Ohio State University ElectroScience Laboratory, Department of Electrical Engineering; prepared under Contract F30602-71-C-0132 for Rome Air Development Center. (RADC-TR-71-248).

3. Carlson, F.P., "Propagation in Stationary and Locally Stationary Random Media," Ph.D. Dissertation, University of Washington, 1967.

4. Zintsmaster, L. R., Report 3163-1, op. cit.

5. Zintsmaster, L. R., Report 3163-1, op. cit.

6. Tatarski, V.I., Wave Propagation in a Turbulent Medium, McGraw-Hill, Chapter 2, 1961 (translated by R.A. Silverman).

7. Zintsmaster, L. R., Report 3163-1, op. cit.

8. Wyngaard, J. C., Izumi, Y., Collins, S.A., J.O.S.A., 61, pp. 1646-1650 (1971).

9. Dungey, W. H., Tarazano, D. O., Wyngaard, J. C., "Meteorogogical Measurements of Turbulence Characteristics," J.O.S.A., 61 (1971) A1552.

III. OUTER SCALE EFFECTS IN TURBULENCE DEGRADED LIGHT BEAM SPECTRA

A. Introduction

This section extends temporal spectrum calculations to include outer scale effects. Log-amplitude, phase, and phase difference spectra are considered for both plane and spherical waves.

Temporal frequency spectra are useful for two distinct reasons. The first is that it is much easier to instrument time spectral measurements because data need be taken at only one point. The corresponding spatial correlations or spatial spectra require measurements at many pairs of points. The second reason is that temporal correlations and spectra are in themselves useful quantities to compare with theoretical estimates to gain information about atmospheric turbulence parameters. In this context they do not suffer from aperture averaging effects as do spatial measurements because readily available time lags are large enough to represent spatial separations much larger than those conveniently available. Thus they provide a good handle with which to examine outer scale effects.

The work presented here parallels Tatarski's (Tatarski, 1967) and Clifford's (Clifford, 1971) calculations of temporal spectra. The new feature is the inclusion of a spatial spectrum that contains the outer scale. The resulting equations are sufficiently similar to those already given that final limiting expressions can be obtained with a minimum of mathematical development.

In the next section, the calculations will be outlined. The spherical wave case will first be considered, expressions for log-amplitude, phase and phase difference spectra being derived. This will be followed by similar derivations for the plane wave case. In both cases the starting equations will be given along with basic results. Expressions for limiting cases are tabulated. In subsequent sections the results are discussed and conclusions drawn.

B. Calculations

To outline the calculations, we first assume Taylors frozen turbulence hypothesis so that when spatial separation ρ and wind velocity v are collinear the temporal and spatial correlations, respectively, $R_{x,s}(\tau)$ and $B_{x,s}(\rho)$ for a path of length, L, are related (Clifford, 1971) by

$$(1a)\quad R_{x,s}(\tau) = \int_0^L \frac{d}{dz}\left(B_{x,s}\left(\frac{v\tau L}{z}\right)\right)dz$$

for spherical waves and (Tatarski, 1967)

(1b) $R_{x,s}(\tau) = B_{x,s}(v\tau)$

for the plane wave case. The subscripts x and s refer to log-amplitude and phase respectively.

Equations (1a) and (1b) show how large separation (ρ) turbulence statistics may be obtained by using the time lagged data from a moderately long record at one point. Further the temporal phase difference correlation $R_{\delta s}(\tau)$ is given by

(2a) $R_{\delta s}(\tau) = \langle [s(r,t) - s(r+\rho,t)][s(r-v\tau,t) - s(r+\rho-v\tau,t)] \rangle$

For a plane wave this reduces to

(2b) $R_{\delta s}(\tau) = 2B_s(v\tau) - B_s(v(\tau-\rho/v) - B_s(v(\tau+\rho/v))$

and for a spherical wave

$$(2c)\quad R_{\delta s}(\tau) = \int_0^L \frac{d}{dz} \left\{ 2B_s\left(\frac{v\tau L}{z}\right) - B_s\left(\frac{vL}{z}\left(\tau - \frac{\rho z}{vL}\right)\right) - B_s\left(\frac{vL}{z}\left(\tau + \frac{\rho z}{vL}\right)\right)\right\} dz .$$

Following previous work the temporal spectrum (Tatarski, 1967) is given by

$$(3)\qquad W_{x,s}(f) = 4 \int_0^\infty d\tau \cos(2\pi f\tau) R_{x,s}(\tau) .$$

For the spherical wave case the log-amplitude (upper sign) and phase (lower sign) correlation functions are given by

$$(4)\qquad B_{x,s}(\rho) = 2\pi^2 k^2 \int_0^L dz \int_0^\infty d\kappa\, \kappa \Phi_n(\kappa)\, J_0\left(\frac{\kappa\rho z}{L}\right)\left\{1 \mp \cos\left[\frac{\kappa^2 z(L-z)}{kL}\right]\right\}$$

where $\lambda = 2\pi/k$ is the light wavelength. The index spectrum (Tatarski, 1961) to be used is

$$(5) \qquad \Phi(\kappa) = 0.033\, C_n^2 \left\{ \left(\frac{1.077}{L_o} \right)^2 + \kappa^2 \right\}^{-11/6}$$

where L_o is the turbulence outer scale. The value of 1.077 for the coefficient of $1/L_o$ was chosen to give two limiting forms for the index structure function

$$(6) \qquad D_n(\rho) = \begin{cases} C_n^2 \rho^{2/3} & \rho << L_o \\ C_n^2 L_o^{2/3} & \rho >> L_o \end{cases}$$

so that on a log-log plot of $D_n(\rho)$ the break point determined by the intersection of the asymptotic forms occurs precisely at $\rho = L_o$.

Following previous work (Clifford, 1971) Eqs. (5), (4), (1a) are substituted into Eq. (3) and the τ integration is performed. The derivation is continued by substituting

$$(7a) \quad z/L = (u+1)/2$$

and

$$(7b) \quad \sigma' = \{(\kappa v/2\pi\rho)^2 - 1\}\beta^{-2}$$

where

$$(7c) \quad \beta^2 = 1 + (1.077 v/2\pi f L_o)^2$$

and

$$(7d) \quad \Omega = 2\pi f L^{1/2}/k^{1/2} v$$

and performing the σ' integration in a fashion following that of Reference 1. The result is

$$(8) \quad W_{x,s} = .132\pi^{5/2} k^{2/3} C_n^2 L^{7/3} v^{-1} \Omega^{-8/3} \beta^{-8/3} (\Gamma(4/3)/\Gamma(11/6)$$

$$\times \mathrm{Re} \int_0^1 du \left(1 \mp \exp[-i\Omega^2(u^2-1)/4] \right) \{ {}_1F_1(1/2; -1/3; i\beta^2\Omega^2(u^2-1)/4)$$

$$+ (\Gamma(-4/3)\Gamma(11/6)/\pi^{1/2}\Gamma(4/3)(i\beta^2\Omega^2(u^2-1)/4)^{4/3}$$

$${}_1F_1(11/6; 7/3; i\beta^2\Omega^2(u^2-1)/4).$$

$$(5) \qquad \Phi(\kappa) = 0.033\, C_n^2 \left\{ \left(\frac{1.077}{L_o} \right)^2 + \kappa^2 \right\}^{-11/6}$$

where L_o is the turbulence outer scale. The value of 1.077 for the coefficient of $1/L_o$ was chosen to give two limiting forms for the index structure function

$$(6) \qquad D_n(\rho) = \begin{cases} C_n^2 \rho^{2/3} & \rho << L_o \\ C_n^2 L_o^{2/3} & \rho >> L_o \end{cases}$$

so that on a log-log plot of $D_n(\rho)$ the break point determined by the intersection of the asymptotic forms occurs precisely at $\rho = L_o$.

Following previous work (Clifford, 1971) Eqs. (5), (4), (1a) are substituted into Eq. (3) and the τ integration is performed. The derivation is continued by substituting

$$(7a) \quad z/L = (u+1)/2$$

and

$$(7b) \quad \sigma' = \{(\kappa v/2\pi\rho)^2 - 1\}\beta^{-2}$$

where

$$(7c) \quad \beta^2 = 1 + (1.077 v/2\pi f L_o)^2$$

and

$$(7d) \quad \Omega = 2\pi f L^{1/2}/k^{1/2} v$$

and performing the σ' integration in a fashion following that of Reference 1. The result is

$$(8) \quad W_{x,s} = .132\pi^{5/2} k^{2/3} C_n^2 L^{7/3} v^{-1} \Omega^{-8/3} \beta^{-8/3} (\Gamma(4/3)/\Gamma(11/6)$$

$$\times \mathrm{Re} \int_0^1 du \left(1 \mp \exp[-i\Omega^2(u^2-1)/4] \right) \{ {}_1F_1(1/2; -1/3; i\beta^2\Omega^2(u^2-1)/4)$$

$$+ (\Gamma(-4/3)\Gamma(11/6)/\pi^{1/2}\Gamma(4/3)(i\beta^2\Omega^2(u^2-1)/4)^{4/3}$$

$${}_1F_1(11/6; 7/3; i\beta^2\Omega^2(u^2-1)/4).$$

where

$$(9a) \qquad {}_1F_1(a;b;x) = \frac{\Gamma(b)}{\Gamma(a)} \sum_{n=0}^{\infty} \frac{\Gamma(a+n)}{\Gamma(b+n)} \frac{x^n}{n!}$$

$$(9b) \qquad = \Gamma(b)\left\{ \frac{e^{-i\pi a}\, x^{-a}}{\Gamma(b-a)} \sum_{n=0}^{\infty} \frac{\Gamma(a+n)\Gamma(1+a-b+n)}{\Gamma(a)\,\Gamma(1+a-b)n!}(-x)^{-n} \right.$$

$$\left. + \frac{e^x x^{a-b}}{\Gamma(a)} \sum_{n=0}^{\infty} \frac{\Gamma(b-a+n)}{\Gamma(b-a)} \frac{\Gamma(1-a+n)}{\Gamma(1-a)} \frac{x^{-n}}{n!} \right\};$$

$$-\frac{\pi}{2} < \arg(x) < \frac{3\pi}{2}$$

Equation (8) is given because it is easily manipulated to give asymptotic forms. Note that the new information is in the factor β which contains the outer scale. Indeed Eq. (8) reduces to the corresponding equation in the appendix of (Clifford, 1971) if the outer scale becomes infinite.

Using Eqs. (9) to expand the functions in Eq. (8) in a power series in (u^2-1) and using the standard series expansion for e^x, we integrate with respect to u to obtain the limiting forms for large and small Ω shown in Table I. The expansions have been carried out to a number of terms sufficient to indicate the predominant behavior. Again if $\beta = 1$ the expressions of (Clifford, 1971) result.

The spherical phase difference spectrum is obtained by following a similar procedure. Inserting Eqs. (5), (4) and (2c) into Eq. (3) and performing the τ integration gives

$$(10) \quad W_{\delta s}(f) = 0.264\pi^2 k^{2/3} L^{7/3} C_n^2 v^{-1} \Omega^{-8/3} \beta^{-8/3} \cdot \int_0^1 du \left[1-\cos\left(\frac{\pi\rho f u}{v}\right)\cos\frac{\pi\rho f}{v}\right]$$

$$\cdot \int_0^{\infty} \frac{d\sigma' \sigma'^{-1/2}}{(\sigma'+1)^{11/6}} \left\{1+\cos\left[-\Omega^2(\sigma'\beta^2+1)\frac{(1-u^2)}{4}\right]\right\}$$

where Eqs. (7) are used to convert to the new variables. With the exception of the β factor, this term is identical with Eq. (20) of (Clifford, 1971). Since $\beta \gtrsim 1$ the arguments given in that Reference for dropping the second integral are still valid with the result that $W_{\delta s}(f)$ has the form given in Table I for large and small f.

TABLE I

The Limiting Case Results for Plane and Spherical Wave Time Spectra with Outer Scale as a Parameter

$$\Omega \equiv f/f_o; \quad f_o \equiv \frac{v}{\sqrt{2\pi\lambda L}}; \quad \beta^2 \equiv \left(1 + \left(\frac{1.077v}{2\pi f L_o}\right)^2\right)$$

PLANE WAVE

log amplitude

$$\Omega\beta<<1 \quad W_\chi(f) = .850\, C_n^2 k^{2/3} L^{7/3} v^{-1} (1-[1.45\beta^{4/3} - 1.29\beta^{-2/3} - .430\beta^{-8/3}]\Omega^{4/3})$$

$$\Omega\beta>>1 \quad W_\chi(f) = 2.19\, C_n^2 k^{2/3} L^{7/3} v^{-1} (\Omega\beta)^{-8/3}$$

phase

$$\Omega\beta<<1 \quad W_s(f) = 4.38\, C_n^2 k^{2/3} L^{7/3} v^{-1} (\Omega\beta)^{-8/3} (1-.194(\Omega\beta)^{+8/3})$$

$$\Omega\beta>>1 \quad W_s(f) = 2.19\, C_n^2 k^{2/3} L^{7/3} v^{-1} (\Omega\beta)^{-8/3}$$

phase difference

$$\rho<< (\lambda L)^{1/2} \quad W_{\delta s}(f) = \left\{\begin{matrix}.033\\.066\end{matrix}\right\} C_n^2 k^2 L v^{5/3} \left[1 - \cos\left(\frac{2\pi\rho f}{v}\right)\right] \beta^{-8/3} f^{-8/3}$$

$$\rho>> (\lambda L)^{1/2}$$

SPHERICAL WAVE

log amplitude

$$\Omega\beta<<1 \quad W_\chi(f) = .191\, C_n^2 k^{2/3} L^{7/3} v^{-1} (1-[.645\beta^{4/3} - .573\beta^{-2/3} - .191\beta^{-8/3}]\Omega^{4/3})$$

$$\Omega\beta>>1 \quad W_\chi(f) = 2.19\, C_n^2 k^{2/3} L^{7/3} v^{-1} (\Omega\beta)^{-8/3}$$

phase

$$\Omega\beta<<1 \quad W_s(f) = 4.38\, C_n^2 k^{2/3} L^{7/3} v^{-1} (\Omega\beta)^{-8/3} [1 - .0436(\Omega\beta)^{8/3}]$$

$$\Omega\beta>>1 \quad W_s(f) = 2.19\, C_n^2\, k^{2/3} L^{7/3} v^{-1} (\Omega\beta)^{-8/3}$$

phase difference

$$\rho<< (\lambda L)^{1/2} \quad W_{\delta s}(f) = \left\{\begin{matrix}.033\\.066\end{matrix}\right\} C_n^2 k^2 L v^{5/3} \left[1 - \frac{\sin\left(\frac{2\pi\rho f}{v}\right)}{\left(\frac{2\pi\rho f}{v}\right)}\right] \beta^{-8/3}\, f^{-8/3}$$

$$\rho>> (\lambda L)^{1/2}$$

For the plane wave case, the log-amplitude (upper sign) and phase (lower sign) correlation functions are given by

$$(11)\quad B_{x,s}(\rho) = 2\pi^2 k^2 L \int_0^\infty d\kappa\, \kappa\, J_0(\kappa\rho)\left\{1 \mp \frac{k}{\kappa^2 L}\sin\left(\frac{\kappa^2 L}{k}\right)\right\}\Phi_n(\kappa)$$

Substituting Eqs. (11), (5) and (1b) into (3), performing the τ integration and substituting Eqs. (7c) and (7d) and

$$(12)\qquad z = \Omega^2((\kappa v/2\pi f)^2 - 1)$$

gives

$$(13)\quad W_{x,s}(f) = .033\pi^2 k^{2/3} L^{7/3} C_n^2 v^{-1} \int_0^\infty dz\, z^{-1/2}\left[1 \mp \frac{\sin(z+\Omega^2)}{(z+\Omega^2)}\right](z+\beta^2\Omega^2)^{-11/6}$$

A convenient closed form for the z integration has not been found, it can be put into a form useful for limiting cases by employing

$$(14)\qquad \frac{\sin(x+a)}{(x+a)} = \int_0^1 db\, \cos\Big(b\,(x+a)\Big)$$

in Eq. (13) and performing the z integration to yield

$$W_{x,s}(f) = .033\pi^{5/2} k^{2/3} L^{7/3} C_n^2 \Gamma(4/3)\Gamma^{-1}(11/6)\Omega^{-8/3}\beta^{-8/3}\cdot$$

$$(15)\qquad \cdot\left[1 \mp \mathrm{Re}\int_0^1 db\, e^{ib\Omega^2}\left\{{}_1F_1\left(\frac{1}{2};\,-\frac{1}{3};\,-ib\beta^2\Omega^2\right)\right.\right.$$

$$\left.\left. + \Gamma(-4/3)\Gamma(11/6)\Gamma^{-1}(4/3)\pi^{-1/2}(-ib\Omega^2\beta^2)^{4/3}\,{}_1F_1(11/6;7/3;-ib\beta^2\Omega^2)\right\}\right]$$

Employing the series forms for the hypergeometric functions given in Eqs. (9) for large and small Ω then gives the expressions quoted in Table I.

The plane wave phase difference spectrum is obtained quite simply by inserting Eq. (2b) into Eq. (3) and using the shifting theorem., for a real even function. The result is

$$(16)\quad W_{\delta s}(f) = 2\left[1 - \cos\left(\frac{2\pi\rho f}{v}\right)\right]W_s(f)$$

Equation (16) is also used in finding entries for Table I.

C. Discussion

A comparison of two limiting values for each temporal spectrum in Table I reveals that only the log-amplitude has a significant change in form in going from one limiting case to the other. For the time lagged phase and power phase difference spectra, the change from one limiting expression to the other would probably be undetectable experimentally.

The main point of interest in the inclusion of outer scale effects into the temporal spectrum calculations is the effect on low frequency behavior. To this end the low frequency limits associated with the expressions given in Table I have been extracted, and are presented in Table II. They apply for the case where $f << 1.077v/2\pi L_o$, i.e., the period of the frequency being measured is greater than the time required for the turbulence field to traverse a distance of one outer scale. (Extremely long averaging times or sophisticated data processing schemes may be required in some cases to obtain such data.) In any case, an interesting point is that the log-amplitude and phase spectra approach a constant limit.

The spherical wave phase difference spectrum is of special interest because it is being measured at RADC. It may be put into a convenient nondimensional form by using dimensionless variable combinations. The form is

$$\left(\frac{2\pi f\rho}{v}\right)_s\left(\frac{1.077\rho}{L_o}\right) \text{ and } \frac{W_{\delta s}(f)}{N k^2 L\, C_n^2\, \rho^{5/3}} \text{ to yield}$$

$$(17)\quad \left(\frac{W_{\delta s}(f)}{k^2 L\, C_n^2\, \rho^{5/3}}\right) = \left(\frac{\rho}{v}\right)\left(\frac{2\pi f\rho}{v}\right)^{-8/3}\left[1 - \frac{\sin\left(\frac{2\pi f\rho}{v}\right)}{\left(\frac{2\pi f\rho}{v}\right)}\right]$$

$$\left(1 + \frac{\left(\frac{1.077\rho}{L_o}\right)^2}{\left(\frac{2\pi f\rho}{v}\right)^2}\right)^{-4/3} \cdot \qquad N = 0.033\,(2\pi)^{8/3}\left\{\begin{matrix}1\\2\end{matrix}\right\} \approx 4.44\left\{\begin{matrix}1\\2\end{matrix}\right\}$$

Figure 1 is a log-log plot of Eq. (17) when $\rho << L_o$. The initial slope is +2 until the 1st break point of $\frac{2\pi f\rho}{v} = \frac{1.077\rho}{L_o}$ where the slope is -2/3. The slope then becomes -8/3 after the 2nd break point of $\frac{2\pi f\rho}{v} = \sqrt{6}$.

TABLE II

Low Frequency Asymptotic Results $f << \frac{1.077v}{2\pi L_o}$

PLANE WAVE

Log Amplitude

$$\sqrt{\lambda L} << L_o \quad W_\chi(f) = .850 C_n^2 k^{2/3} L^{7/3} v^{-1} \left[1 - \left(\frac{1.077}{L_o}\right)^{4/3} \left(\frac{L}{k}\right)^{2/3} \left\{1.45 - 1.29\left(\frac{2\pi f L_o}{1.077v}\right)^2 - .430\left(\frac{2\pi f L_o}{1.077v}\right)^4\right\}\right]$$

$$\sqrt{\lambda L} >> L_o \quad W_\chi(f) = 2.19 C_n^2 k^2 L\, v^{-1} \left(\frac{L_o}{1.077}\right)^{8/3}$$

Phase

$$\sqrt{\lambda L} << L_o \quad W_s(f) = 4.38 C_n^2 k^2 L\, v^{-1} \left(\frac{L_o}{1.077}\right)^{8/3} \left[1 - .194\left[\left(\frac{1.077}{L_o}\right)^2 \frac{L}{k}\right]^{4/3}\right]$$

$$\sqrt{\lambda L} >> L_o \quad W_s(f) = 2.19 C_n^2 k^2 L\, v^{-1} \left(\frac{L_o}{1.077}\right)^{8/3}$$

Phase difference

$$\rho << \sqrt{\lambda L} \quad \rho >> \sqrt{\lambda L} \quad W_{\delta s}(f) = \left\{\begin{matrix} 4.44 \\ 8.87 \end{matrix}\right\} C_n^2 k^2 L v^{-1} \left(\frac{L_o}{1.077}\right)^{8/3} \left[1 - \cos\left(\frac{2\pi\rho f}{v}\right)\right]$$

SPHERICAL WAVE

Log Amplitude

$$\sqrt{\lambda L} << L_o \quad W_\chi(f) = .191 C_n^2 k^{2/3} L^{7/3} v^{-1} \left[1 - \left(\frac{1.077}{L_o}\right)^{4/3} \left(\frac{L}{k}\right)^{2/3} \left\{.645 - .573\left(\frac{2\pi f L_o}{1.077v}\right)^2 - .191\left(\frac{2\pi f L_o}{1.077v}\right)^4\right\}\right]$$

$$\sqrt{\lambda L} >> L_o \quad W_\chi(f) = 2.19\, C_n^2 k^2 L v^{-1} \left(\frac{L_o}{1.077}\right)^{8/3}$$

Phase

$$\sqrt{\lambda L} << L_o \quad W_s(f) = 4.38\, C_n^2 k^2 L v^{-1} \left(\frac{L_o}{1.077}\right)^{8/3} \left[1 - .0436\left[\left(\frac{1.077}{L_o}\right)^2 \frac{L}{k}\right]^{4/3}\right]$$

$$\sqrt{\lambda L} >> L_o \quad W_s(f) = 2.19\, C_n^2 k^2 L v^{-1} \left(\frac{L_o}{1.077}\right)^{8/3}$$

Phase difference

$$\rho << \sqrt{\lambda L} \quad \rho >> \sqrt{\lambda L} \quad W_{\delta s}(f) = \left\{\begin{matrix} 4.44 \\ 8.87 \end{matrix}\right\} C_n^2 k^2 L v^{-1} \left(\frac{L_o}{1.077}\right)^{8/3} \left[1 - \frac{\sin\left(\frac{2\pi\rho f}{v}\right)}{\left(\frac{2\pi\rho f}{v}\right)}\right]$$

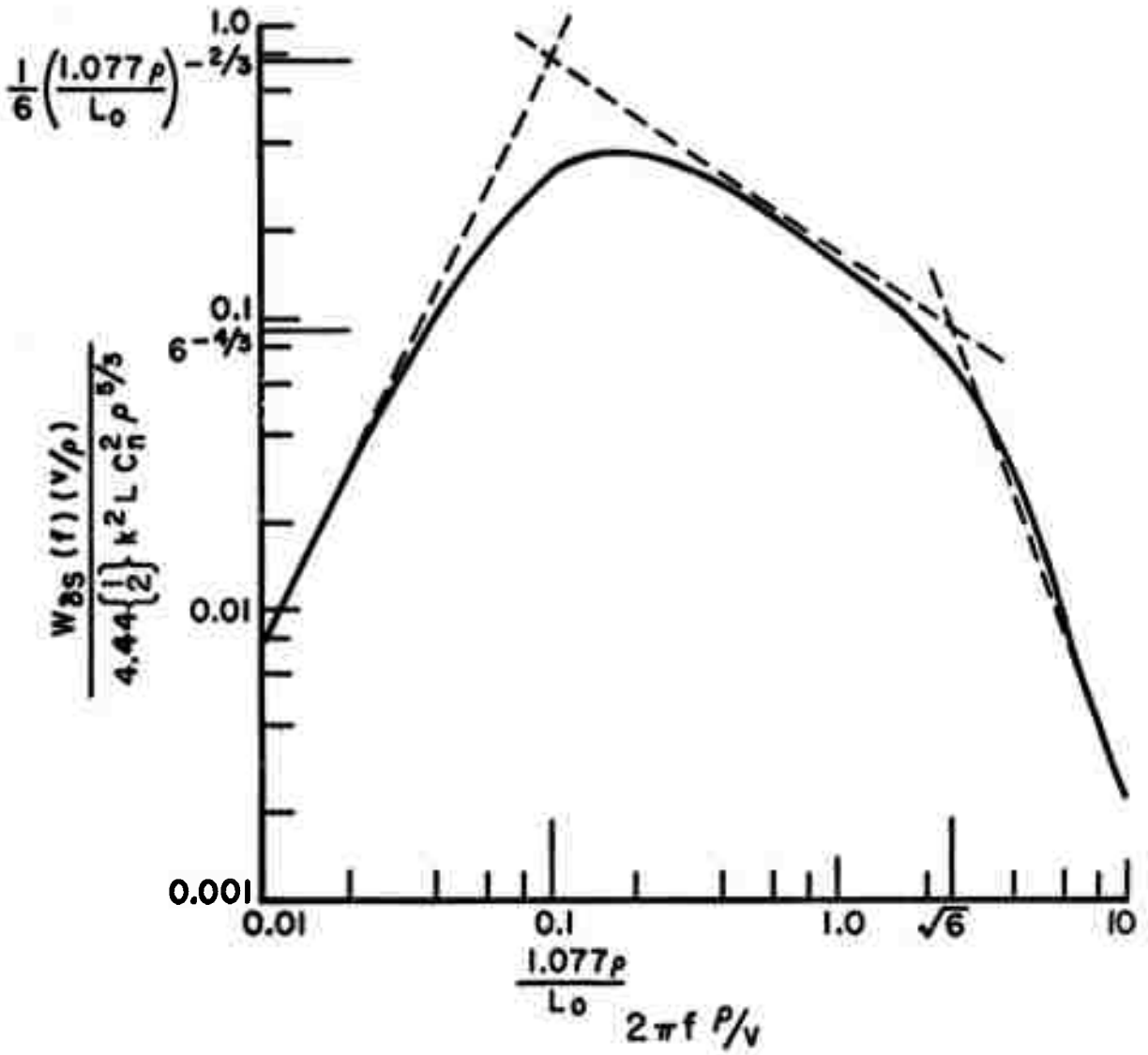

Fig. 1. Normalized phase difference spectra vs normalized separation when the wind direction is parallel to the separation.

D. Conclusions

The previously published temporal spectra for infinite outer scale have been directly extended to finite outer scales thereby verifying the conclusion that outer scale effects only become important when the period of the temporal frequency under consideration is comparable with or longer than the time it takes the wind to move the turbulence one outer scale length. For low temporal frequencies an additional outer scale dependent break point is added to the frequency spectra, and hence low frequency temporal spectra can be used to obtain the outer scale as a check of meteorological measurements.

REFERENCES

1. (Clifford, 1971), S.F. Clifford, JOSA 61, 1285 (1971).

2. (Tatarski, 1967), V.I. Tatarski, RASPROSTR ANANIYE VOLN V TURBULENTNDY ATMOSFERE (The Effects of the Clear Turbulent Atmosphere on Wave Propagation), Moscow: NAUCA, Chapter 4, 1967.

3. (Tatarski, 1961), V.I. Tatarski, Wave Propagation in a Turbulent Medium, McGraw-Hill, New York, Eqs. (2.13) and (1.56) 1961 (transl. by R.S. Silverman).

IV. SUMMARY AND CONCLUSIONS

To review, in the final technical report three areas were considered, and one appendix was presented. The areas were averaging times for propagation data, the calculation of predicted results for various slant path measurements and the calculation of expressions for temporal spectra of several propagation functions. The appendix presented a suggested redefinition for the well known coherence length.

In the area of averaging times an examination of some typical RADC propagation data showed that the averaging times were sufficiently long to assure, that for the mean square value, there would be less than ten percent variation between ensemble and time averages and less than ten percent variation between any given average and the stationary value. The design of a real-time averaging-time meter to give required averaging time while data is being recorded was also discussed. Finally the limitations to the averaging time of temporal spectra were considered. It was indicated that the scatter of spectral values is a lesser restriction on averaging time than is the frequency resolution desired.

In the area of slant path calculations, computer evaluated expressions for the phase structure function and angle of arrival correlation functions for spherical waves were presented. These plots show the nonreciprocal effect of the atmosphere on beams propagating upward and downward in the atmosphere. Other curves of the differential path contribution show the exceptionally deleterious effect of the lower atmospheric layer on downward traveling spherical waves, indicating the desirability of avoiding when possible the lower atmospheric layer.

In the study of temporal spectra, expressions given in the literature for spectra of log-amplitude, phase and phase difference of atmospherically degraded beams were extended to include outer scale effects. The results for phase difference spectra indicate for example, a quadratic behavior at low frequencies not heretofore known.

The appendix contains a recommendation that the coherence length, r_o, be redefined in some cases depending on the outer scale. Specifically, when the coherence length is greater than twice the outer scale, it has negligible effect on optical parameters and should not be considered. For values of the coherence length less than twice the outer scale it should be defined as before.

APPENDIX:
COHERENCE LENGTH REDEFINITION

A. Introduction

The coherence length r_o defined originally by Fried (Fried 1967) as a parameter in the wave structure function is extremely useful in discussions of atmospheric effects on optical heterodyne detection, image resolution and focused spot size. Basically it specifies a receiver diameter above which atmospheric turbulence effects rather than aperture diffraction provide the mechanisms limiting signal-to-noise ratio, resolution, etc. of optical systems. For a plane wave over a horizontal path of length L, wavelength $\lambda = 2\pi/k$ and turbulence structure parameter C_n^2, r_o is given by the well known expression $r_o = (6.88/2.91\ k^2 L C_n^2)^{3/5}$.

In the past the coherence length has been defined for turbulence with assumed infinite outer scale. In many applications (say above 10 meters altitude) the size of the outer scale is not a limiting factor since the outer scale is the order of magnitude of the altitude. However for situations very near the ground, i.e., within the first few meters the outer scale may be sufficiently small to have an observable effect on atmospheric optical measurements. It is the object here to review concepts involving r_o and to suggest an extension of the definition to situations where the effects of a finite outer scale might be noted.

In the sections to follow we will first present a review of some of the situations where coherence length is used. This will lead in a natural fashion to an effective receiver aperture diameter. The effective aperture diameter will then be investigated for finite outer scales to show both qualitatively and quantitatively the effect of finite outer scale. Finally a suggested extension of the coherence length definition will be put forth to describe situations where the coherence length is comparable with or greater than the outer scale.

B. Review

We now consider the situations in which the coherence length was defined and applied. In this section an infinite outer scale will be assumed.

Signal-to-Noise Ratio

The coherence length was originally defined (Fried, 1967) in conjunction with the signal-to-noise ratio of an optical heterodyne receiver detecting an atmospherically degraded light beam. The situation comprised an atmospherically degraded beam collinear with a local oscillator beam, both incident on a round photodetector of quantum efficiency η and of diameter D. Then the basic expression for the ensemble average signal-to-noise ratio $\langle S \rangle / N$ was shown to be

$$(1) \qquad \frac{\langle S \rangle}{N} = \left(\frac{\eta}{e}\right) \frac{2}{\pi D^2} \times \left\langle \left| \int E(\bar{r}_1) d\bar{r}_1 \right|^2 \right\rangle$$

where

e = electron charge,

$E(\bar{r}_1)$ = electric field of atmospherically degraded beam at point $\bar{r}_1$ on photodetector surface, and

angular brackets denote ensemble average.

The expression given in Eq. (1) is simplified in Appendix A with the final result

$$(2a) \qquad \frac{\langle S \rangle}{N} = \left(\frac{\eta}{e}\right) \frac{\langle |E|^2 \rangle}{2} \times \frac{\pi}{4} \times \left[8 \int_0^D r \, dr \, \tau(r) \, M(r) \right]$$

where

r = magnitude of separation of two points on detector surface

(2b) $\tau(r)$ = transfer function of circular aperture

$$= \frac{2}{\pi} \left[\cos^{-1}\left(\frac{r}{D}\right) - \frac{r}{D} \sqrt{1 - \left(\frac{r}{D}\right)^2} \right]$$

(2c) $M(r)$ = atmospheric transfer function

$$= \exp\left(-\frac{1}{2} D_w(r) \right)$$

(2d) $D_w(r)$ = wave structure function

$$= A r^{5/3}.$$

The parameter A is defined by Eq. (2d) and will be evaluated subsequently.

In the absence of turbulent fluctuations or in the limit of very small aperture diameters $M(r) \approx 1$ and the signal-to-noise ratio is, (see Appendix A)

$$(3) \qquad \frac{\langle S \rangle}{N} = \frac{\eta}{e} \frac{\langle |E|^2 \rangle}{2} \frac{\pi D^2}{4} .$$

The coherence length was originally defined by examining the case where the aperture diameter, D, is sufficiently large that the aperture transfer function $\tau(r)$ is constant over the range where $M(r)$ has nonzero contributions to the integral in Eq. (1). For that case $\tau(r) \approx \tau(0) = 1$ and the signal-to-noise ratio approaches a constant value of (see Appendix A)

$$(4) \qquad \langle S\rangle/N = \left(\frac{\eta}{e}\right)\frac{\langle|E|^2\rangle}{2}\,\frac{\pi}{4}\times\left(\frac{6.88}{A}\right)^{6/5}$$

To define r_o, require that Eq. (4) has the same form as the undegraded signal-to-noise ratio expression, Eq. (3), except that the aperture diameter, D has been replaced by a new constant r_o given by

$$(5) \qquad r_o = (6.88/A)^{3/5},$$

for a plane wave propagating over a horizontal path (Fried, 1967), $D_w(r) = 2.91k^2LC_n^2r^{5/3}$ and $A=2.91k^2LC_n^2$, giving $r_o = (6.88/2.91k^2LC_n^2)^{3/5}$. Thus r_o is defined to preserve the form for the case of large aperture signal-to-noise ratio. Other geometries are considered in Appendix B.

Equation (2) can be written in a compact form which expresses the general nature of the aperture dependence and the limiting cases. This is done by defining a new quantity, the effective aperture, D_{eff}. The definition of D_{eff} is made so that for small diameters $D_{eff} = D$; for very large apertures $D_{eff} = r_o$. Hence comparing Eqs. (2a) and (3) we obtain, (for an infinite outer scale)

$$(6a) \quad D_{eff} = \left[8\int_0^D r\,dr\;\tau(r)\;M(r)\right]^{1/2}$$

$$(6b) \quad = \left[8\int_0^D r\,dr\;\frac{2}{\pi}\left[\cos^{-1}\left(\frac{r}{D}\right) - \frac{r}{D}\sqrt{1-\left(\frac{r}{D}\right)^2}\right] e^{-\frac{1}{2}\times 6.88\left(\frac{r}{r_o}\right)^{5/3}}\right]^{1/2}$$

The expression for the mean signal-to-noise ratio, expressed in terms of D_{eff} then becomes

$$(7) \qquad \frac{\langle S\rangle}{N} = \left(\frac{\eta}{e}\right)\frac{\langle|E|^2\rangle}{2}\,\frac{\pi D_{eff}^2}{4}$$

so that average signal-to-noise ratio is proportional to the effective aperture area $\pi D_{eff}^2/4$.

D_{eff} expresses quite directly the concept that for infinite outer scale there is little to be gained in signal-to-noise ratio by making the aperture much larger than r_o.

The effective diameter will also be useful in expressing other quantities which depend on the coherence length.

Imaging Resolution

The coherence length, r_o, also comes into the theory of atmospheric imaging (Fried, 1966). Consider light from a point source propagating through a turbulent atmosphere, imaged by a lens of diameter D to a degraded point pattern $I(\bar{r}_2)$ on an image plane a distance d_i away. The two dimensional Fourier transform of the ensemble average of $I(\bar{r}_2)$ expressed in terms of spatial frequency f, and normalized to unity at zero frequency is shown in Appendix C to be $\tau(f)\ M(f)$. The integral of the spatial spectrum is then defined (Fried, 1966) as the resolution, R.

$$(8a)\quad R = \int\int \tau(f)\ M(f)\ d\bar{f}.$$

The resolution is more commonly written by expressing it in terms of an integral over the input or aperture plane (the plane of the lens). In Appendix C it is shown that the spatial frequency, $\bar{f}$, is related to the input aperture coordinate difference, $\bar{r}$, by $\bar{r} = \lambda d_i \bar{f}$, and that Eq. (8a) can be expressed as

$$(8b)\quad R = \frac{2\pi}{(\lambda d_i)^2}\int_0^D \tau(r)\ M(r)\ r\,dr$$

Equation (8b) is in a form which can be immediately expressed in terms of the effective aperture size D_{eff} giving

$$(8c)\quad R = \frac{1}{(\lambda d_i)^2} \times \frac{\pi D_{eff}^2}{4}$$

Thus the resolution is also a function of the effective aperture area.

Strehl Imaging Intensity Ratio

For atmospheric imaging we also consider the Strehl intensity ratio, D, also called the Strehl definition (O'Neill, 1963)

$$(9a)\quad D = \langle I(0)\rangle / I_o(0),$$

which is the ratio of the ensemble average intensity $\langle I(0)\rangle$ in the center of the degraded point image to $I_o(0)$, the intensity in the center of the point image in the absence of atmospheric degradation.

Equation (9a) is expressed in terms of image plane coordinates. In terms of aperture plane coordinates (see Appendix C) it takes on a familiar form

$$(9b)\quad D = \frac{\int_0^D M(r)\tau(r)r\,dr}{\int_0^D \tau(r)r\,dr}$$

in terms of the effective aperture diameter this becomes

$$(9c)\quad D = \left(\frac{D_{eff}}{D}\right)^2 .$$

Thus the Strehl intensity ratio also turns out to be a normalized form of the resolution, R, and a function of the effective aperture diameter.

Imaged Spot Size

One can talk about another quantity in conjunction with atmospheric imaging, the imaged spot size, (Brackey, 1968). That is defined in terms of the ensemble average intensity, $\langle I(\bar{r}_2)\rangle$, of the degraded point image normalized to unity height at the center. The imaged spot size d_o is defined as the diameter of a cylinder of unity height having the same volume as the ensemble intensity surface, as shown in Fig. 1. Thus we have

$$(10a)\quad \frac{\pi d_o^2}{4} = \frac{\iint \langle I(\bar{r}_2)\rangle d\bar{r}_2}{\langle I(0)\rangle}$$

In terms of the aperture plane variables this becomes (see Appendix C)

$$(10b)\quad d_o^2 = \frac{16}{\pi^2} \times \frac{(\lambda d_i)^2}{8\int M(r)\tau(r)r\,dr}$$

and finally in terms of the effective diameter,

$$(10c)\quad d_o = \frac{4\lambda d_i}{\pi D_{eff}} .$$

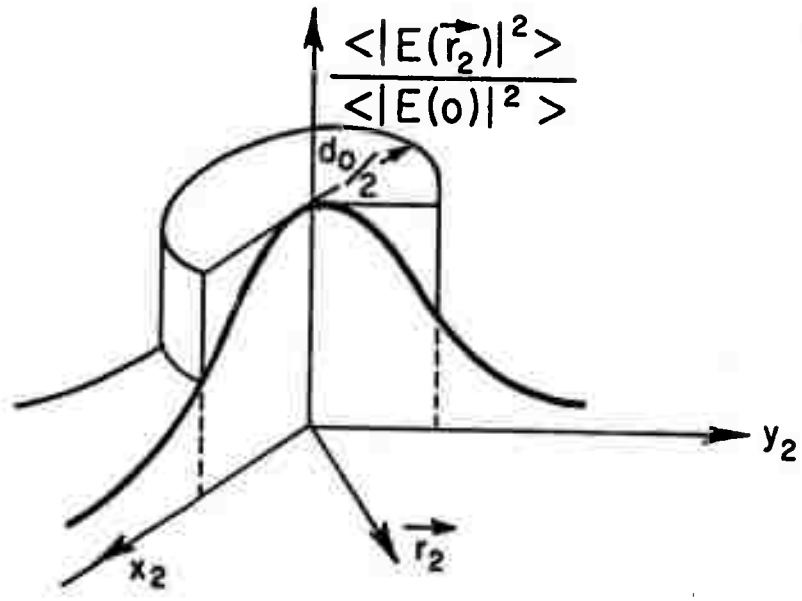

Fig. 1. Illustration of effective spot size definition.

Focused Spot Size

Finally one can consider the size of a spot focussed through the turbulent atmosphere onto a receiving plane. The focused spot size, d_f, can be defined exactly as the imaged spot size in terms of an integral scale of $I(\bar{\rho}_2)$, the intensity in the receiving plane.

$$\frac{\pi d_f^2}{4} = \frac{\iint I(\bar{\rho}_2)\, d\bar{\rho}_2}{I(0)} \tag{11a}$$

It is shown in Appendix D that the expression for $I(\bar{\rho}_2)$ is formally identical with that for the image plane intensity when the image plane distance d_i is replaced by the range, L. The resulting expression for the focussed spot size is then

$$d_f = \frac{4}{\pi}\frac{\lambda L}{D_{eff}} \tag{11b}$$

The ratio of focused to imaged spot sizes d_f/d_0 is then the geometrical magnification $m = d_f/d_0 = L/d_i$ as one would expect.

Thus we see that all the quantities considered can be expressed in terms of the effective aperture diameter. The preceding discussion has treated cases that originated with infinite outer scale. We now want to extend the quantities to the case of finite outer scale. Instead of considering them all separately we will discuss only the behavior of the effective aperture diameter D_{eff} with finite outer scale. The extension to the other quantities is then given by (7), (8c), (9c), (10c) and (11b).

C. Examination of D_{eff}

Having shown that D_{eff} is a unifying factor for the quantities indicated which make use of the coherence length, r_o, we now proceed to examine D_{eff} for cases of finite outer scale. We will show that for outer scale comparable with the coherence length, the behavior of D_{eff} is significantly different, approaching that of the small aperture situation. This will then lead to the recommended extension of the definition of the coherence length. The procedure will be to first examine certain limiting cases for D_{eff} to establish the general behavior and then to consider a few numerical values to illustrate the significant points.

The definition of D_{eff} including outer scale effects will formally be the same as in Eqs. (2) and (6) with the wave structure function extended to include outer scale effects.

$$(12)\quad D_{eff}^2 = 8\int_0^D r\,dr\ \frac{2}{\pi}\left[\cos^{-1}\left(\frac{r}{D}\right) - \frac{r}{D}\sqrt{1-\left(\frac{r}{D}\right)^2}\right] e^{-\frac{1}{2}D_w(r)}$$

Outer scale effects are included by utilizing a turbulence spatial spectrum which includes outer scale effects,

$$(13)\quad \Phi(\kappa) = \frac{0.033\,C_n^2}{\left(\left(\frac{1.077}{L_o}\right)^2 + \kappa^2\right)^{11/6}}$$

This definition was chosen to satisfy two criteria: for $r \ll L_o$, $D_n(r) = C_n^2\, r^{2/3}$, and for $r \gg L_o$, $D_n(r) = C_n^2 L_o^{2/3}$. The factor of 1.077 arises because of the second criterion, as discussed in Appendix E.

The associated wave structure functions for plane and spherical waves are given by Eqs. (14a) and (14b), respectively

$$(14a) \qquad D_{wp}(r) = 8\pi^2 k^2 L \int_0^\infty [1 - J_0(\kappa r)]\Phi_n(\kappa)\kappa \, d\kappa$$

$$(14b) \qquad D_{ws}(r) = 8\pi^2 k^2 \int_0^L d\eta \left(\frac{L}{\eta}\right)^2 \int_0^\infty [1-J_0(\kappa r)]\Phi\left(\frac{\kappa L}{\eta}\right) \kappa \, d\kappa$$

These two functions are plotted in Fig. 2. They have the expected behavior. For small values of r

$$(14c) \qquad D_{ws}(r) = \frac{3}{8} D_{wp}(r) = \frac{3}{8} 2.41 \, k^2 L \, C_n^2 \, r^{5/3}$$

Both of these will be represented by the infinite outer scale expression

$$(14d) \qquad D_{wp,s} = 6.88(r/r_0)^{5/3} = 6.88(r/r_{op,s})^{5/3}$$

where r_{op}, and r_{os} are given in Eqs.(B7) and (B10). For large values of r they both saturate at the same value which is shown in Appendix E to be

$$(14e) \qquad D_{ws,p}(\infty) = 1.381 \, k^2 L C_n^2 \, L_o^{5/3}$$

The fact that the wave variance, $B_w(0) = \frac{1}{2} D_w(\infty)$, was the same for both plane and spherical documents the fact that the mean square log amplitude plus phase fluctuation generated along a single line, connecting transmitter and receiver depends only upon the path and not upon the type of wave either side of the path.

We can now also write the infinite separation value $D_w(\infty)$ in terms of the coherence length for plane and spherical waves, respectively.

$$(15a) \qquad D_{wp}(\infty) = 3.265\left(\frac{L_o}{r_{op}}\right)^{5/3}$$

$$(15b) \qquad D_{ws}(\infty) = 8.71\left(\frac{L_o}{r_{os}}\right)^{5/3}$$

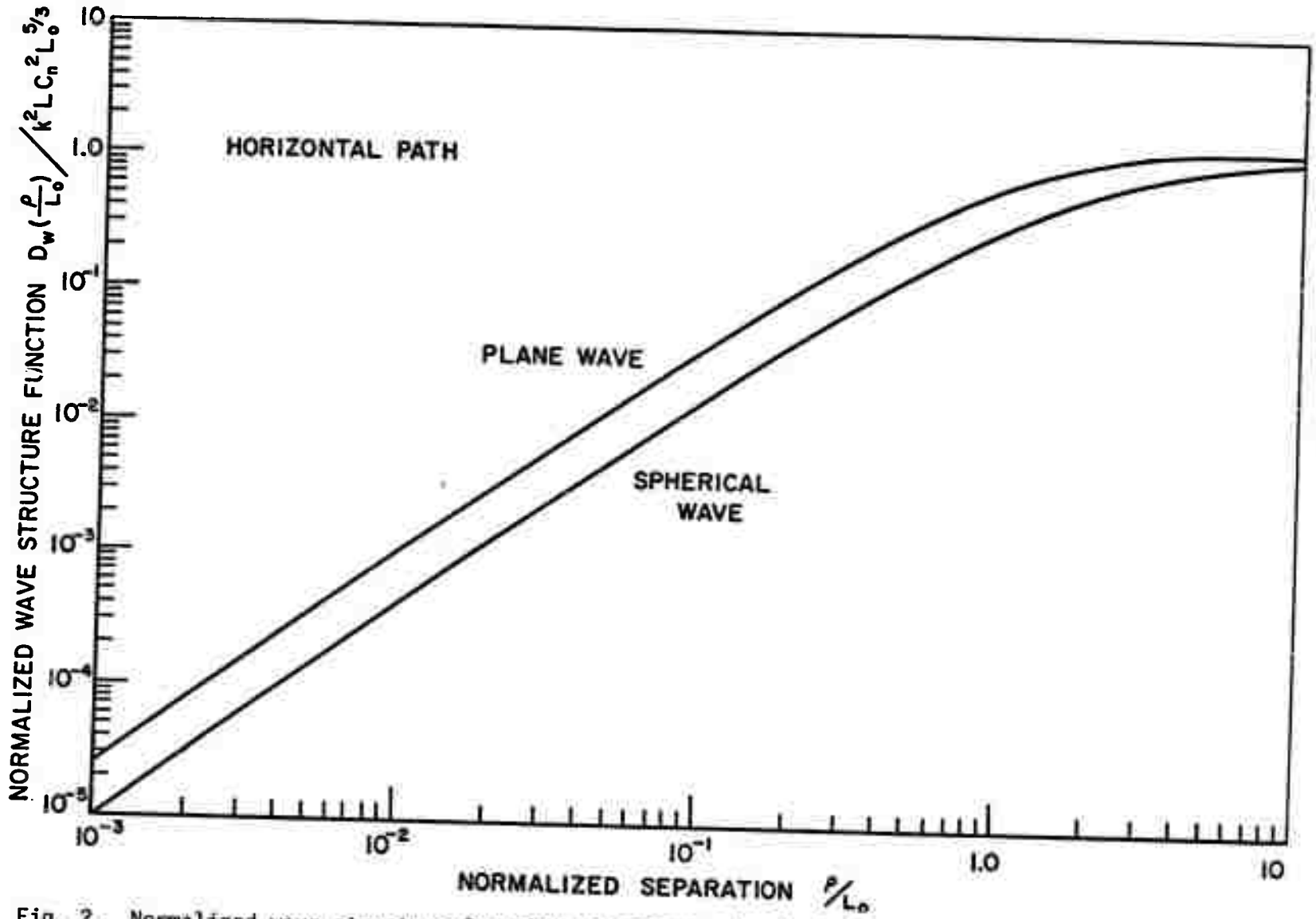

Fig. 2. Normalized wave structure function for plane and spherical waves vs. normalized separation for finite outer scale and horizontal path.

The limiting expressions for D_w will now be used in the calculation of asymptotic forms for the effective diameter.

To provide a feeling for how the effective diameter should behave for various ranges of the actual aperture diameter we qualitatively examine the integral expression, Eq. (11), for the various cases of interest. The procedure will be to sketch curves for the various factors in the integral definition to demonstrate the limiting cases. The two factors of interest are the optical transfer function, $\tau(r) = \frac{2}{\pi} \cos^{-1}\left(\frac{r}{D}\right) - \frac{r}{D}\sqrt{1 - (r/D)^2}$ which goes from 1 at $r = 0$ to 0 at $r = D$ and the atmospheric transfer function $M(r) = \exp\left(-\frac{1}{2} D_w(r)\right)$ which drops off as $\exp\left\{-3.44 \left(\frac{r}{r_o}\right)^{5/3}\right\}$ for $r << L_o$ and assumes the limiting value of $\exp\left\{-\frac{C}{2} (L_o/r_o)^{5/3}\right\}$ for $r >> L_o$. The value of the constant C depends on the type of wave as reflected in Eqs. (15). Sketches of $\tau(r)$ and $M(r)$ are shown in Fig. 3a. From Eqs. (12), the effective diameter is then the square root of area under the curved formed from r times the product of the two curves.

We now sketch the two curves for various ranges of D.

Case I. $D << r_o << L_o$ (see Fig. 3b).

This is the infinite outer scale small aperture case considered in the previous section. $M(r)$ is essentially constant for $0 < r < D$ so that

$$(16a) \qquad D_{eff} \doteq \left[8 \int_0^D dr\, r\, \tau(r)\right]^{1/2} = D.$$

Case II. $r_o << D << L_o$ (see Fig. 3c).

This is the large aperture case considered earlier. $\tau(r)$ is essentially constant over the range where $M(r)$ is significant, so that

$$(16b) \qquad D_{eff} \doteq \left[\frac{2.8}{\pi} \int_0^\infty r dr \exp\left\{-3.44(r/r_o)^{5/3}\right\}\right]^{1/2} = r_o$$

Case III. $D >> r_o >> L_o$ (see Fig. 3d).

This case is new. In this case $M(r)$ drops to an asymptotic value before $\tau(r)$ goes to zero so that

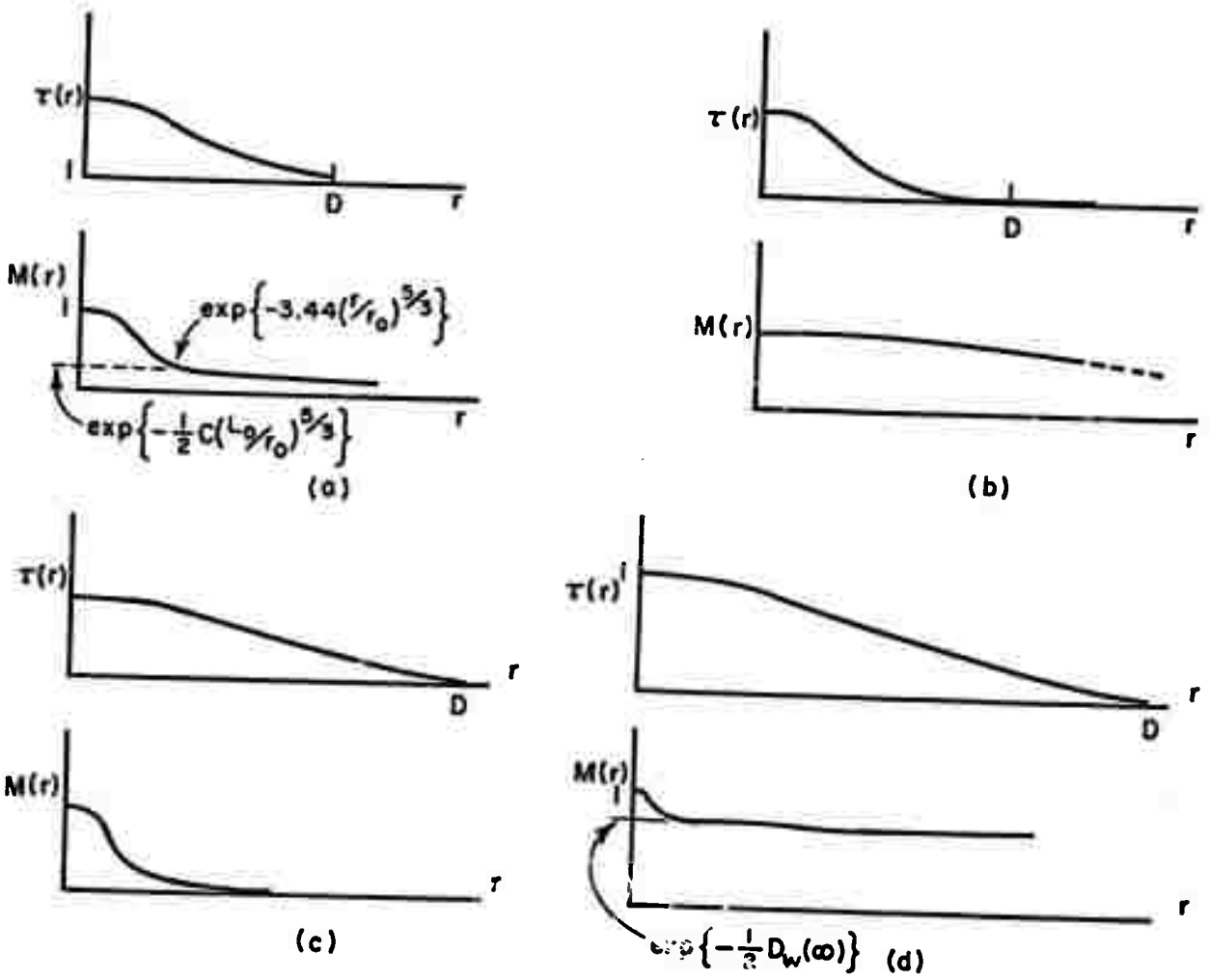

Fig. 3. Graphs illustrating behavior of functions determining D_{eff} for various ratios of r_0, L_0, and D.

(17a) $$M(r) \approx \exp\{-\tfrac{1}{2} C(L_o/r_o)^{5/3}\}$$

over almost all of the range $0 \leq r \leq D$ and

(17b) $$D_{eff} \approx [\exp\{-\tfrac{1}{2} C(L_o/r_o)^{5/3}\} \times 8 \int_0^D dr\, r\, \tau(r)]^{1/2}$$

$$= D \exp\{-\tfrac{1}{4} C(L_o/r_o)^{5/3}\} = D \exp\{-\tfrac{1}{4} D_w(\infty)\} .$$

Thus D_{eff} is again proportional to D, this time the constant of proportionality being $\exp(-1/4\ D_w(\infty))$. These three regions are shown in the log-log sketch of D_{eff} vs D in Fig. 4.

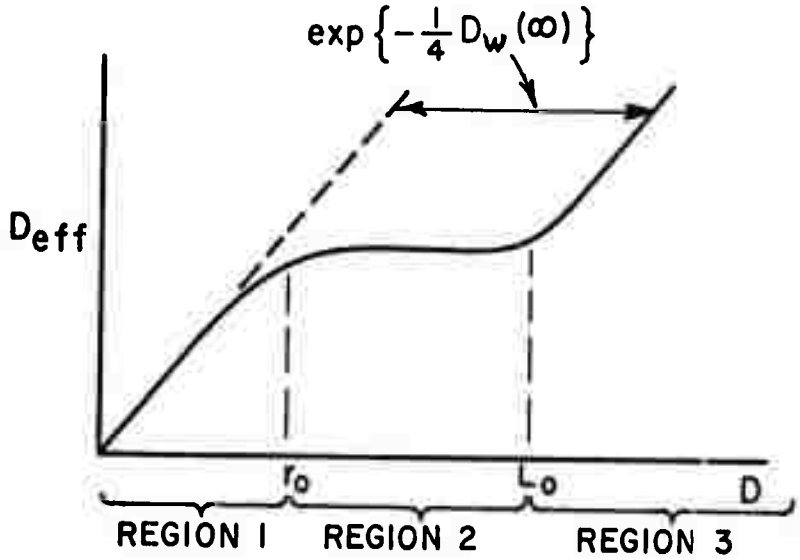

Fig. 4. Sketch of D_{eff} vs D showing various regions.

The significant point here is in the behavior in region III. For small values of the ratio L_o/r_o the sidestep as determined from the factor $\exp\{-\ C/4\ (L_o/r_o)^{5/3}\}$ is negligible and the line in region III is a continuation of the line in region I. For that case the behavior is no different from the infinite outer scale case discussed in the first section. However, for larger values of L_o/r_o, the line in region III is sidestepped significantly and the behavior in the two regions is different.

The difference in the two regions is indicated by the amount of sidestep obtained from the expression $\exp\{-\ C/4\ (L_o/r_o)^{5/3}\}$. This quantity is plotted as a function of L_o/r_o in Fig. 5 for both plane and spherical waves. There we see that for L_o equal to r_o the sidestep is 1/0.4 = 2.5 for plane waves. (Actually the factor $\exp\{-\ C/4\ (L_o/r_o)^{5/3}\}$

gives a change in the vertical position which is then translated into a sidestep of $1/\exp\{-C/4\,(L_o/r_o)^{5/3}\}$. The corresponding value for spherical waves is 1/0.10 for spherical waves. For the outer scale one half the coherence length, the straight line portions in regions I and III of the D_{eff} vs D graph should be within a factor of 2.5 of each other for both plane and spherical waves. This will be used in the next section where a suggested extension of the definition of the outer scale will be presented.

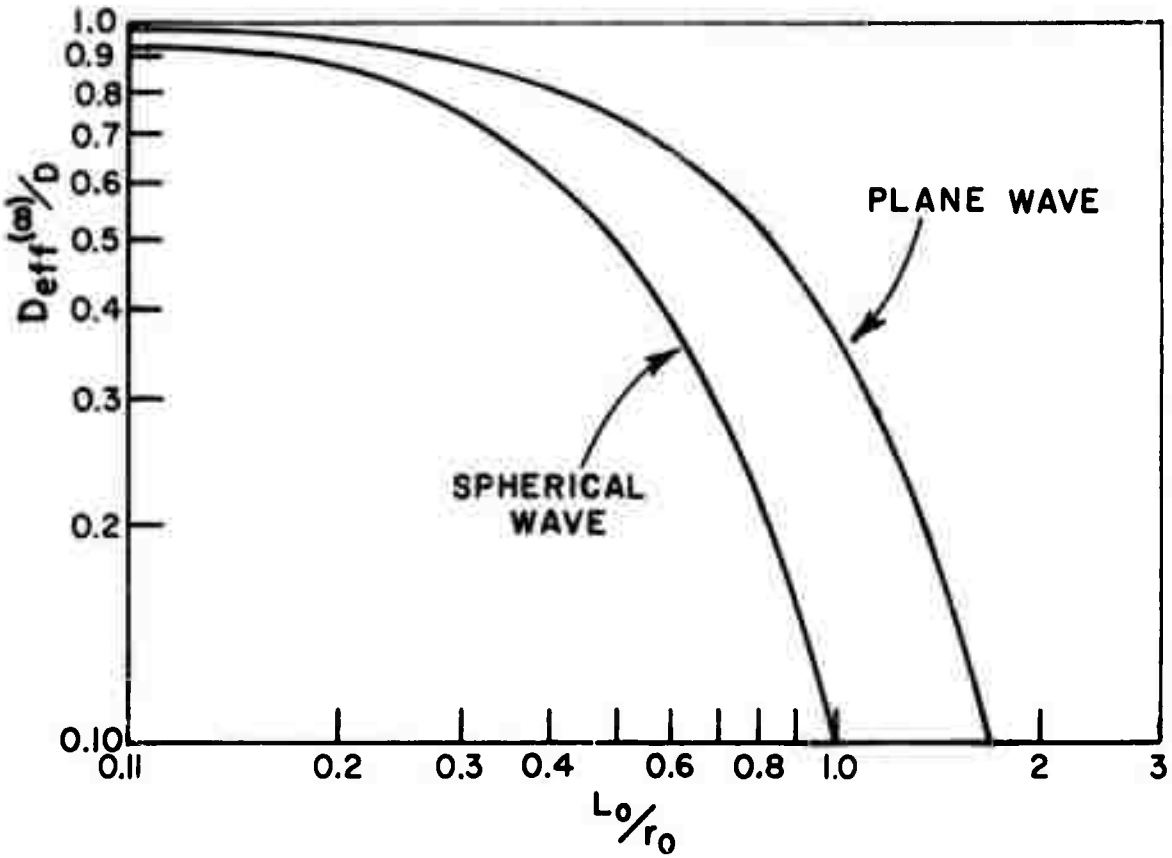

Fig. 5. Graph of effective diameter D_{eff} vs L_o/r_o for plane and spherical waves.

D. Extension of the Definition of r_o

In the previous section we examined the limiting cases of the behavior of the effective diameter as a function of outer scale and coherence length, and noted that with finite but large outer scale, D_{eff} saturates at the value r_o as it did with infinite outer scale. Indeed with outer scale less than half the coherence length, the curve of D_{eff} versus D would show less than a factor of two variation in going from D less than L_o to D greater than L_o. This behavior is indicated more clearly in Fig. 6 where we see computed plots of D_{eff} vs D covering the range of D much less than L_o to much greater than L_o

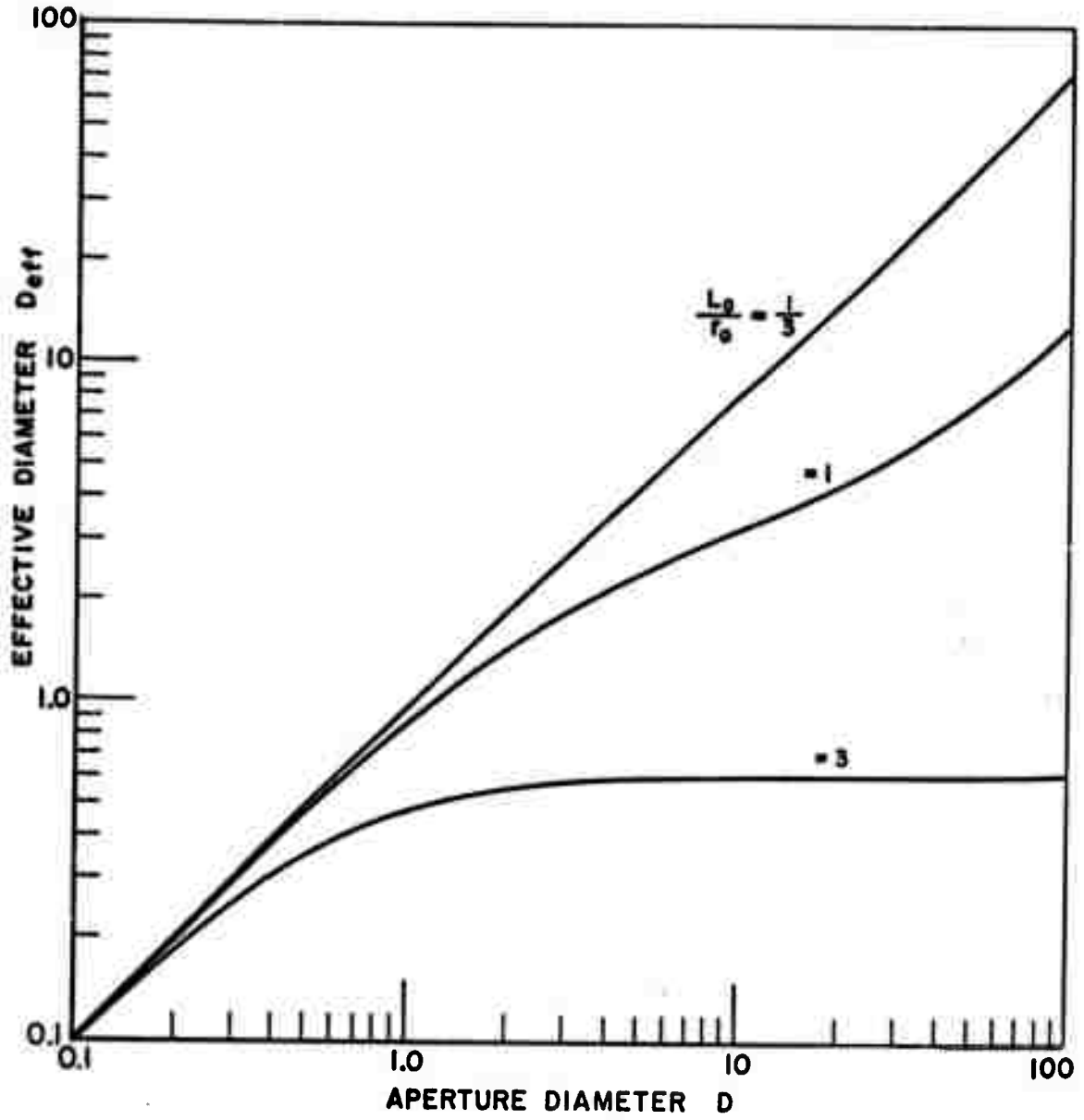

Fig. 6. Effective aperture diameter D_{eff} vs actual diameter for various values of ratio outer scale to coherence length (L_0/r_0), for a spherical wave.

for several ratios of L_o/r_o. We see that for $L_o/r_o \leq 1$ the transition from one straight line portion of the D_{eff} versus D curve to the other is nearly undetectable. Therefore a representative generalization when $L_o/r_o \leq 1$ is that the D_{eff} versus D curve is essentially the no turbulence case, where $D_{eff} = D$.

Thus it is recommended that the coherence length not be defined for cases of outer scale less than one half the coherence length, and that for cases with outer scale greater than one half the coherence length the definition of coherence length for infinite outer scale be retained. This extension is the formal embodiment of the fact that the coherence length is a useful quantity for $r_o < L_o$ but that for $r_o > L_o$ the behavior is essentially that of the no-turbulence case.

E. Discussion

There are a few loose ends yet to pick up. The first is a discussion of the physical behavior for the $r_o > L_o$ case. Basically the meaning is contained in the wave variance $B_w(0) = .69\ k^2\ LC_n^2\ L_o^{5/3}$ which is the maximum value of $D_w(r)/2$. In terms of $B_w(0)$ the largest ratio of D_{eff}/D is $\exp(-1/2\ B_w(0))$. When the maximum phase variance is less than 0.5 rad^2, i.e., 0.707 rad RMS deviation or less than a quarter wave, then the optical effects of the atmosphere are essentially negligible. In such a case the resolution will be unimparied. For such a case a quantity which measures the atmospheric resolution degradation will cease to have its full meaning and can be safely neglected.

F. Summary and Conclusions

In this appendix we have considered the effects of atmospheric turbulence on optical heterodyne detection and on optical resolution and spot size. Specifically we considered the case when the outer scale of turbulence is comparable with the coherence length, r_o, and suggested an extension of the definition of the coherence length.

First the heterodyne signal-to-noise ratio and the imaging quantities were shown to all be functions of the effective aperture diameter, a quantity which, for infinite outer scale, is equal to the aperture diameter for very small apertures, and is equal to the coherence length for very large diameters.

The effective aperture diameter was then investigated for finite outer scales. It was found that when the outer scale was small enough to be less than one half the coherence length that the effective aperture diameter varied with actual diameter essentially as if there were no turbulence. Thus it is recommended that when the outer scale of turbulence was less than half the coherence length that the coherence length be undefined and that when the outer scale is larger than the coherence length that the usual definition of coherence length apply!

REFERENCES

Brackey, T.A., (1968), "Preliminary Report on the Use of Spatial Diversity in Optical Communications Systems," Report 2156-9, 10 April 1968, The Ohio State University ElectroScience Laboratory, Department of Electrical Engineering; prepared under Contract BPSN No. 7-68406202, and AF 33(615)-3419, Air Force Avionics Laboratory, Air Force Systems Command, Wright-Patterson Air Force Base, Ohio.

deWolf, D.A., (1971), "Effects of Turbulence Instabilities on Laser Propagation," Advanced Research Projects Agency, No. 1379, October 1967.

Fried, D.L., (1966), "Optical Resolution Through a Randomly Inhomogeneous Medium for Very Long and Very Short Exposures," J. Opt. Soc. Am. 56, 1372-1379, October 1966.

Fried, D.L., (1967), "Optical Heterodyne Detection of an Atmospherically Distorted Signal Wave," Proc. IEEE 55, 57-67, January 1967.

O'Neill, E.L., (1963), Introduction to Statistical Optics, Addison-Wesley Publishing Co., Inc., p. 87.

Tatarski, V.I., (1961), Wave Propagation in a Turbulent Medium, (Translated by R.A. Silverman), McGraw-Hill Book Co., (1961).

APPENDIX A

In this appendix are presented the steps necessary to reduce Eq. (1) to Eq. (2) and to examine certain limiting cases. Writing the ensemble average square of the integral in Eq. (1) as a double integral and exchanging integrations and summation gives

$$(A1)\quad \left\langle \left| \int E(\bar{r}_1)\, d\bar{r}_1 \right|^2 \right\rangle = \left\langle \iint_{\text{aperture}} E(\bar{r}_1')\, E^*(\bar{r}_1'')\, d\bar{r}_1\, d\bar{r}_1'' \right\rangle$$

$$= \iint_{\text{aperture}} \langle E(\bar{r}_1')E^*(\bar{r}_1'')\rangle d\bar{r}_1' d\bar{r}_1'' .$$

Switch to sum and difference coordinates $\bar{r} = \overline{r_1' - r_1''}$ and $\bar{R} = \overline{(r_1' + r_1'')}/2$. Using the definition of the atmospheric mutual coherence function, (Fried, 1967),

$$(A2)\quad \langle E(\bar{r}_1')E^*(\bar{r}_1'')\rangle = \langle |E|^2 \rangle\, M(|\bar{r}_1' - \bar{r}_1''|) = \langle |E|^2 \rangle\, M(\bar{r}),$$

and using the aperture function $f(\bar{r}_1)$, given by

$$(A3)\quad f(\bar{r}_1) = \begin{cases} 1; & |\bar{r}_1| \le D \\ 0; & |\bar{r}_1| > D , \end{cases}$$

we have

$$(A4)\quad \left\langle \left| \int E(\bar{r}_1)\, d\bar{r}_1 \right|^2 \right\rangle = \int\int\int\int_{-\infty}^{\infty} f(\bar{r}_1')\, f(\bar{r}_1'') \langle E(\bar{r}_1')E^*(\bar{r}_1'')\rangle\, d\bar{r}_1' d\bar{r}_1''$$

$$(A5)\quad = \langle |E|^2 \rangle \iint_{-\infty}^{\infty} d\bar{r} M(r) \left[\iint_{-\infty}^{\infty} d\bar{R}\, f\left(\bar{R} + \frac{\bar{r}}{2}\right) f\left(\bar{R} - \frac{\bar{r}}{2}\right) \right].$$

The inner integral is related to the aperture transfer function $\tau(r)$ by

$$(A6)\quad \iint_{-\infty}^{\infty} d\bar{R}\, f\left(\bar{R} + \frac{\bar{r}}{2}\right) f\left(\bar{R} - \frac{\bar{r}}{2}\right) \equiv \tau(r) \iint_{-\infty}^{\infty} d\bar{R}\, f(\bar{R}) = \frac{\pi D^2}{4}\, \tau(r)$$

For a circular aperture

$$\tau(r) = \frac{2}{\pi}\left[\cos^{-1}\left(\frac{r}{D}\right) - \frac{r}{D}\sqrt{1-\left(\frac{r}{D}\right)^2}\right] \tag{A7}$$

Inserting Eq. (A6) into Eq. (A5) gives

$$\left\langle\left|\int E(\bar{r}_1)d\bar{r}_1\right|^2\right\rangle = \langle|E|^2\rangle \frac{\pi D^2}{4}\int_{-\infty}^{\infty}\int d\bar{r}\, M(r)\tau(r) \tag{A8}$$

Since $M(r)$ and $\tau(r)$ are functions of r, magnitude of $\bar{r}$, we switch to polar coordinates and perform the angular integration, giving

$$\left\langle\left|\int E(\bar{r}_1)d\bar{r}_1\right|^2\right\rangle = \langle|E|^2\rangle \frac{\pi^2 D^2}{2}\int r\, dr\, M(r)\,\tau(r). \tag{A9}$$

Equation (A9) is the desired result. Inserting Eq. (A9) into Eq. (1) gives Eq. (1b)!

Equation (A9) can be examined for two limiting cases. For aperture diameters small compared with the coherence length $M(r)$ is constant over the region of interest and

$$\left\langle\left|\int E(\bar{r}_1)d\bar{r}_1\right|^2\right\rangle = \langle|E|^2\rangle \frac{\pi^2 D^2}{2}\int_0^D \bar{r}\, d\bar{r} \times \frac{2}{\pi}\left[\cos^{-1}\left(\frac{r}{D}\right) - \frac{r}{D}\sqrt{1-\left(\frac{r}{D}\right)^2}\right] \tag{A10}$$

$$= \langle|E|^2\rangle \left(\frac{\pi D^2}{4}\right)^2 \tag{A11}$$

This is used in the derivation of Eq. (2).

For aperture diameter, D, much larger than the coherence length, $\tau(r) = 1$ over the region of interest, and Eq. (A9) becomes

$$\left\langle\left|\int E(\bar{r}_1)d\bar{r}_1\right|^2\right\rangle = \langle|E|^2\rangle \frac{\pi^2 D^2}{2}\int r\, dr\, e^{-\frac{1}{2}Ar^{5/3}} \tag{A12}$$

$$= \langle|E|^2\rangle \frac{\pi^2 D^2}{2} \times \left(\frac{2}{A}\right)^{6/5} \times \frac{3}{5}\Gamma(6/5) \tag{A13}$$

(A14) $$= \frac{\langle |E|^2 \rangle \pi^2 D^2}{2} \frac{}{8} \times \left(\frac{2 \times 3.44}{A} \right)^{6/5}$$

Equation (A14) is used in the derivation of Eq. (4).

APPENDIX B

In this appendix we present general expressions for coherence length for plane and spherical waves for cases where C_n^2 is a function of range. First consider the plane wave case

$$(B1) \qquad D_w(r) = 8\pi^2 k^2 \int_0^L dz \int_0^\infty d\kappa\ \kappa\Phi_n(\kappa)\ [1 - J_o(\kappa\rho)]$$

Taking

$$(B2) \qquad \Phi(k) = 0.33 C_n^2(z)\kappa^{-11/3}$$

and making the substitutions

$$(B3) \qquad u = \kappa\rho$$

and

$$(B4) \qquad v = z/L$$

gives

$$(B5) \qquad D_w(r) = .033 \times 8\pi^2 k^2 L r^{5/3} \int_0^1 dv\ C_n^2(vL) \int_0^\infty du\ u^{-8/5}\ [1 - J_o(u)]\ .$$

Further, from Eqs. (2d) and (5) of the main text.

$$(B6) \qquad D_w(r) = 6.88 \left(\frac{r}{r_o}\right)^{5/3}$$

Using known values for the u integral, (Tatarski, 1961, p. 269) and solving for r_o gives the desired results

$$(B7a) \qquad r_o = \left[\frac{6.88}{2.91\ k^2 L \int_0^1 dv\ C_n^2(Lv)}\right]^{3/5}$$

and when C_n^2 is a constant

$$(B7b) \qquad r_o = \left[\frac{6.88}{2.91\ k^2\ L\ C_n^2}\right]^{3/5}$$

For a spherical wave

$$(B8) \qquad D_w(\rho) = 8\pi^2 k^2 \int_0^L dz \left(\frac{L}{z}\right)^2 \int_0^\infty d\kappa\, \kappa \Phi_n\left(\kappa\, \frac{L}{z}\right)\left[1 - J_o(\kappa\rho)\right]$$

substituting for $\Phi(\kappa)$ from Eq. (B2), for κ and z from (B3) and (B4) respectively, and simplifying gives

$$(B9) \qquad D_w(\rho) = 0.033 \times 8\pi^2 k^2 L \rho^{5/3} \int_0^1 dv\, v^{5/3}\, C_n^2(Lv) \int_0^\infty du[1-J_o(u)]u^{-8/3}$$

Evaluating the u integral and solving for r_o using Eq. (B6) gives

$$(B10a) \qquad r_o = \left[\frac{6.88}{2.91\, k^2 L \int_0^1 du\, u^{5/3}\, C_n^2(Lu)}\right]^{3/5}$$

and when C_n^2 is a constant

$$(B10b) \qquad r_o = \left[\frac{6.88}{(2.91)\times(3/8)\, k^2 L\, C_n^2}\right]^{3/5}$$

Equations (B7) and (B10) are the last results of this appendix, general formulas for the coherence length, (r_o) when C_n^2 is a function of longitudinal position.

APPENDIX C

In this appendix we present derivations of several expressions for imaging situations. The first is the derivation relating the normalized Fourier transformation of the image plane intensity $I(\bar{r}_2)$ to the spectrum $\tau(f)M(f)$ and also to the integral over the input aperture in Eq. (6b). The spectrum of the image plane intensity is given by

$$P(f) = \iint e^{i2\pi \bar{f}\cdot\bar{r}_2} \langle I(\bar{r}_2)\rangle \, d\bar{r}_2 \, . \tag{C1}$$

In Eq. (C1) $\bar{f}$ is spatial frequency in cycles per meter.

The image plane intensity is related to the input plane fields by the well known relationship

$$\langle I(\bar{r}_2)\rangle = \left(\frac{k}{2\pi d_i}\right)^2 \left\langle \left| \iint E(\bar{r}_1)\, e^{i\frac{k}{d_i}\bar{r}_1\cdot\bar{r}_2} \, d\bar{r}_1 \right|^2 \right\rangle \tag{C2}$$

$$= \left(\frac{k}{2\pi d_i}\right)^2 \iint d\bar{r}_1 \iint d\bar{r}_1'' \langle E(\bar{r}_1')E^*(\bar{r}_1'')\rangle \, e^{i\frac{k}{d_i}(\bar{r}_1'-\bar{r}_1'')\cdot\bar{r}_2} \tag{C3}$$

Following steps identical to those in Appendix A we switch to the same sum and difference coordinates, express $\langle E(\bar{r}_1')E(\bar{r}_1'')\rangle$ in terms of the atmospheric transfer function, and perform the integration over the sum coordinate, $\bar{R}$. The result is comparable to Eq. (A8) and reduces to Eq. (A8) for $\bar{r}_2 = 0$. The result is

$$\langle I(\bar{r}_2)\rangle = \left(\frac{k}{2\pi d_i}\right)^2 \langle |E|^2\rangle \frac{\pi D^2}{4} \iint d\bar{r}\, \tau(r)\, M(r)\, e^{i\frac{k}{d_i}\bar{r}\cdot\bar{r}_2} \tag{C4}$$

Inserting this expression for $I(\bar{r}_2)$ into Eq. (C1) and performing the $\bar{r}_2$ integration gives

$$P(f) = \left(\frac{k}{d_i}\right)^2 \langle |E|^2\rangle \frac{\pi D^2}{4} \int_{-\infty}^{\infty}\int d\bar{r}\, \tau(r)M(r)\delta\left(2\pi\bar{f} + \frac{k}{d_i}\bar{r}\right) \tag{C5}$$

We note that $P(0)$ can be easily evaluated since $M(0) = \tau(0) = 1$. The result is

$$P(0) = \langle |E|^2\rangle \frac{\pi D^2}{4} \tag{C6}$$

Performing the $\bar{r}$ integration in Eq. (C5) and normalizing the result to $P(0)$ gives one desired result, the form of the normalized transform of $I(\bar{r}_2)$:

$$\frac{P(f)}{P(0)} = \tau(\lambda d_i f)\, M(\lambda d_i f). \tag{C6}$$

The integral expression for the resolution can be quite easily obtained by integrating Eq. (C5) with respect to $\bar{f}$ and noting that $\bar{f}$ occurs only in the delta function. The result for

$$\iint \frac{P(f)}{P(0)} d\bar{f}$$

is

$$R = \iint \frac{P(f)}{P(0)}\, d\bar{f} = \left(\frac{k}{2\pi d_i}\right)^2 \iint d\bar{r}\ \tau(r)M(r) \tag{C7}$$

$$= \frac{2\pi}{(\lambda d_i)^2} \int_0^D r\, dr\ \tau(r)\, M(r) \tag{C8}$$

Eq. (C8) is another desired result.

To obtain the aperture plane expression for the Strehl intensity ratio, we use Eq. (C4) and simplify by performing the angular $\bar{r}$ integration. The result is

$$D = \frac{I(0)}{I_o(0)} = \frac{2\pi \int rdr\ \tau(r)M(r)}{2\pi \int rdr\ \tau(r)} \tag{C9}$$

To obtain the imaged spot diameter as defined in Eq. (10a) we use Eq. (C4). Thus since $\tau(0) = M(0) = 1$

$$\int \langle I(\bar{r}_2)\rangle\, d\bar{r}_2 = \langle |E|^2 \rangle \frac{\pi D^2}{4} \tag{C10}$$

and

$$\langle I(0)\rangle = \left(\frac{k}{2\pi d_2}\right)^2 \langle |E|^2 \rangle \frac{\pi D^2}{4} \iint d\bar{r}\ \tau(r)M(r) \tag{C11}$$

(C12) $$= \left(\frac{k}{2\pi d_2}\right)^2 \langle |E|^2 \rangle \ \frac{\pi D^2}{4} \ \times 2\pi \int r dr \ \tau(r) M(r)$$

Inserting Eqs. (C10) and (C11) into Eq. (10a) and rearranging gives Eq. (10b) the desired result.

APPENDIX D

In this appendix we consider a light beam that is focused through a turbulent atmosphere to a beam waist. An expression is derived for the focused spot size in that situation. The development parallels that of deWolf (deWolf, 1971) but the definition is one which reduces to proper values in the case of vanishing turbulence and finite aperture.

Let the transmitting aperture and observation planes be designated respectively by transverse coordinates $\bar{\rho}_1$ and $\bar{\rho}_2$ and longitudinal values z_1 and z_2. Then assuming the limitations of Fresnel diffraction, $E_2(\bar{\rho}_2)$ the field at the observation plane is given by

$$(D\text{-}1) \qquad E_2(\bar{\rho}_2) = + \frac{ik\, e^{-ik\left(L + \frac{\rho_2^2}{2L}\right)}}{2\pi L} \iint d\bar{\rho}_1\, E(\bar{\rho}_1)\, \exp\left(\frac{ik\rho_1^2}{2R}\right)$$

$$\cdot \exp\left(\frac{-ik}{2L}\left(\rho_1^2 - 2\bar{\rho}_1 \cdot \bar{\rho}_2\right)\right) B(\bar{\rho}_1, \bar{\rho}_2)$$

where

(D-1b) $E(\bar{\rho}_1)\exp(-ik\rho_1^2/2L)$ is the transmitting aperture plane field

(D-1c) $L = z_2 - z_1$

(D-1c) $B(\bar{\rho}_1, \bar{\rho}_2)$ = modification to Greens function due to turbulent atmosphere.

The ensemble average irradiance pattern, $I(\rho_2)$ in the focal plane, R=L

$$(D\text{-}2) \qquad I(\rho_2) = \langle |E_2(\bar{\rho}_2)|^2 \rangle =$$

$$\left(\frac{k}{2\pi L}\right)^2 \iiiint d\bar{\rho}_1 d\bar{\rho}_1'\, E(\bar{\rho}_1) E^*(\bar{\rho}_1')\, e^{\frac{ik}{L}\,\bar{\rho}_2 \cdot (\bar{\rho}_1 - \bar{\rho}_1')} \langle B(\bar{\rho}_1, \bar{\rho}_2) B^*(\bar{\rho}_1', \bar{\rho}_2) \rangle$$

Assuming an isotropic reciprocal atmosphere (DeWolf, 1971), $\langle B(\bar{\rho}_1, \bar{\rho}_2)\, B^*(\bar{\rho}_1', \bar{\rho}_2) \rangle$ is the spherical wave atmospheric transfer function

$$(D\text{-}3) \qquad \langle B(\bar{\rho}_1, \bar{\rho}_2)\, B^*(\bar{\rho}_1', \bar{\rho}_2) \rangle = M(|\bar{\rho}_1' - \bar{\rho}_2|) = \exp(-\tfrac{1}{2} D_{ws}(|\bar{\rho}_1 - \bar{\rho}_1'|)$$

where $D_{ws}(|\bar{\rho}_1 - \bar{\rho}_1'|)$ is the spherical wave structure function.

Writing Eq. (D3) in terms of sum and difference coordinates

(D-4a) $$\bar{r} = \bar{\rho}_1 - \bar{\rho}_1'$$

(D-4b) $$\bar{R} = \frac{\bar{\rho}_1 + \bar{\rho}_1'}{2}$$

gives

(D5) $$I(\rho_2) = \left(\frac{k}{2\pi L}\right) \iint d\bar{r}\, e^{-\frac{1}{2}D_{ws}(r) + \frac{ik}{L}\bar{\rho}_2 \cdot \bar{r}}$$

$$\times \iint d\bar{R}\, E_1(\bar{R} + \frac{\bar{r}}{2})\, E_1^*(\bar{R} - \frac{\bar{r}}{2})$$

The inner integral is related to the aperture transfer function, $\tau(\bar{r})$. For the usual case of a round aperture of diameter D illuminated by light of constant intensity, $|E_1|^2$, the inner integral is given in Eq. (A-5) by

(D-6) $$\iint d\bar{R}\, E_1(\bar{R} + \frac{\bar{r}}{2})\, E_1^*(\bar{R} - \frac{\bar{r}}{2}) = |E_1|^2 \frac{\pi D^2}{4} \times \tau(r)$$

where $\tau(r)$ is the aperture transfer function

(D-7) $$\tau(r) = \frac{2}{\pi}\left\{\cos^{-1}\left(\frac{r}{D}\right) - \frac{r}{D}\sqrt{1 - \left(\frac{r}{D}\right)^2}\right\}$$

and

(D-8) $$I(\rho_2) = \left(\frac{b}{2\pi L}\right)^2 \left(\frac{\pi D^2}{4}\right) |E_1|^2 \int d\bar{r}\, M(r)\, \tau(r)\, e^{\frac{ik}{L}\bar{\rho}_2 \cdot \bar{r}}$$

The focused spot size is defined by the normalized integral scale as was the imaged focused spot size (see Appendix A)

(D-9) $$\frac{\pi d_1^2}{4} = \frac{\iint I(\rho_2) d\bar{\rho}_2}{I(0)}$$

This definition has the advantage that it is applicable to gaussian beams as well as evenly illuminated apertures, and reduces to the standard finite well definied value for an evenly illuminated aperture in the absence of turbulence.

Equation (D-9) is simply evaluated by noting that Eq. (D-8) is formally identical with Eq. (C-4) if we interchange $\underline{\rho}_2$ and $\underline{r}_2$ and d_i and L and that the numerator and denominator of Eq. (D-9) have been evaluated in Eqs. (C-10) and (C-12) respectively. The resulting expression for Eq. (D-9) is

$$(D\text{-}10) \qquad d_f = \frac{4\lambda L}{\pi D_{eff}}$$

Thus we see that D_{eff} also determines the size of a spot focused through turbulence. We note also that the ratio of the imaged spot size to the focused spot size is m, where

$$m = \frac{d_o}{d_f} = \frac{d_i}{L} .$$

m is merely the geometrical magnification as one might expect.

APPENDIX E

In this appendix we present the integrals which determine the numerical constants in the Von Karmann index spectrum. Let us assume that the spectrum has the form

$$\text{(E-1)} \qquad \Phi_n(\kappa) = C_n^2 \, A/((B/L_o)^2 + \kappa^2)^{11/6}$$

κ is the magnitude of the three-dimensional spatial frequency. We determine the constants A and B by the requirements placed on the associated structure function, $D_n(r)$

$$\text{(E-2)} \qquad D_n(r) = C_n^2 \, r^{2/3} \qquad r << L_o$$

$$\text{(E-3)} \qquad D_n(r) = C_n^2 \, L_o^{2/3} \qquad r >> L_o$$

This choice is made so that on a log-log plot of $D_n(r)$ vs r, then extensions of these asymptotic lines intersect at $r=L_o$ giving the effective breakpoint at that value.

For an isotropic spectrum, the spectrum and structure function are related by

$$\text{(E-4)} \qquad D_n(r) = 8\pi \int_0^\infty \left(1 - \frac{\sin \kappa r}{\kappa r}\right) \Phi(\kappa) \kappa^2 d\kappa$$

Inserting Eq. (E-1) into Eq. (E-4) and making approximation (E-2) gives

$$\text{(E-5)} \qquad C_n^2 r^{2/3} = 8\pi \, C_n^2 \, A \int_0^\infty \left(1 - \frac{\sin \kappa r}{\kappa r}\right) \kappa^{-5/3} \, d\kappa.$$

Using (Tatarski, 1961, p. 270), we have

$$\text{(E-6)} \qquad C_n^2 \, r^{2/3} = 8\pi \, C_n^2 \, A r^{2/3} \times \pi/2\Gamma \, (8/3) \sin \, (\pi/3)$$

where $\Gamma(x)$ is the gamma function. Thus we have

$$\text{(E-7)} \qquad A = \Gamma\left(\frac{8}{3}\right) \sin \frac{\pi}{3} \, / \, 4\pi^2 = 0.033$$

Again inserting Eq. (E-1) into Eq. (E-4) and making approximations (E-3) gives

$$(E\text{-}8) \qquad C_n^2 L_o^{5/3} = C_n^2 \, 8\pi \, A \int_0^\infty \frac{\kappa^2 d\kappa}{((B/L_o)^2 + \kappa^2)^{11/6}} \quad .$$

Using (Gradshteyn, 1965, Eq. 3.251-2)

$$(E\text{-}9) \qquad = C_n^2 \, 8\pi A \, B^{-2/3} \, L_o^{2/3} \, \frac{1}{2} B\left(\frac{3}{2}, \frac{1}{3}\right) = C_n^2 \, 8\pi A \, B^{-2/3} L_o^{2/3} \, \frac{\frac{1}{2}\Gamma\left(\frac{3}{2}\right)\Gamma\left(\frac{1}{3}\right)}{\Gamma(11/6)}$$

where $B(x,y)$ is the Beta function. Using the identity $\Gamma(z)\Gamma(1-z) = \pi \csc \pi z$, we find

$$(E\text{-}10) \qquad B = \left\{ \frac{5}{9} \frac{\Gamma\left(\frac{1}{2}\right)}{\Gamma\left(\frac{11}{6}\right)} \right\}^{3/2} = 1.077.$$

The final result is

$$(E\text{-}11) \qquad \Phi_n(\kappa) = \frac{0.033 \, C_n^2}{\left(\left(\frac{1.077}{L_o}\right)^2 + \kappa^2\right)^{11/6}} \quad .$$

Now consider the plane and spherical wave structure functions for finite outer scale and large separation. From Eq. (B-1) we have for a plane wave

$$(E\text{-}12) \qquad D_{w,p\ell}(\rho) = 8\pi^2 k^2 \int_0^L dz \int_0^\infty d\kappa \, \kappa \Phi_n(\kappa) \, [1 - J_o(\kappa\rho)]$$

and from Eq. (B-8) for a spherical wave

$$(E\text{-}13) \qquad D_{w,sp}(\rho) = 8\pi^2 k^2 \int_0^L \left(\frac{L}{z}\right)^2 dz \int_0^\infty d\kappa \, \kappa \Phi_n\left(\kappa \frac{L}{z}\right)\left[1 - J_o(\kappa\rho)\right]$$

Substituting $\kappa' = \kappa$ in Eq. (E-12) and $\kappa' = \kappa L/z$ in Eq. (E-13) and letting ρ be large so that $J_o(\kappa\rho) \ll 1$ gives the same expression for both equations, it is

$$(E\text{-}14) \qquad D_w(\infty) = 8\pi^2 k^2 \int_0^L dz \int_0^\infty d\kappa' \, \kappa' \, \Phi_n(\kappa')$$

Substituting for $\Phi_n(\kappa)$ from Eq. (E-11) and performing the integrals gives for both plane and spherical waves

$$(E\text{-}15) \qquad D_w(\infty) = \frac{4\pi^2 \times 0.033 \times (6/5)k^2}{(1.077)^{5/3}} \, L \, C_n^2 \, L_o^{5/3}$$

$$= 1.381.$$

This value is quoted in Eq. (14e) of the text.